

Structural and diagenetic control of fluid migration and cementation along the Moab fault, Utah

Peter Eichhubl, Nicholas C. Davatzes, and Stephen P. Becker

ABSTRACT

The Moab fault, a basin-scale normal fault that juxtaposes Jurassic eolian sandstone units against Upper Jurassic and Cretaceous shale and sandstone, is locally associated with extensive calcite and lesser quartz cement. We mapped the distribution of fault-related diagenetic alteration products relative to the fault structure to identify sealing and conductive fault segments for fluid flow and to relate fault–fluid-flow behavior to the internal architecture of the fault zone. Calcite cement occurs as vein and breccia cement along slip surfaces and as discontinuous vein cement and concretions in fault damage zones. The cement predominates along fault segments that are composed of joints, sheared joints, and breccias that overprint earlier deformation bands. Using the distribution of fault-related calcite cement as an indicator of paleofluid migration, we infer that fault-parallel fluid flow was focused along fault segments that were overprinted by joints and sheared joints. Joint density, and thus fault-parallel permeability, is highest at locations of structural complexity such as fault intersections, extensional steps, and fault-segment terminations. The association of calcite with remnant hydrocarbons suggests that calcite precipitation was mediated by the degradation and microbial oxidation of hydrocarbons. We propose that the discontinuous occurrence of microbially mediated calcite cement may impede, but not completely seal, fault-parallel fluid flow. Fault-perpendicular flow, however, is mostly impeded by the juxtaposition of the sandstone units against shale and

AUTHORS

PETER EICHHUBL ~ *Bureau of Economic Geology, Jackson School of Geosciences, University of Texas at Austin, Texas 78758; peter.eichhubl@beg.utexas.edu*

Peter Eichhubl received his M.S. degree from the University of Vienna, Austria, and his Ph.D. from the University of California, Santa Barbara. After research positions at Stanford University and the Monterey Bay Aquarium Research Institute, he joined the Bureau of Economic Geology at the University of Texas in Austin in 2006. His research interests include the interaction of brittle deformation and diagenesis, and fault and fracture mechanics.

NICHOLAS C. DAVATZES ~ *Department of Geology, Temple University, Philadelphia, Pennsylvania 19122*

Nicholas C. Davatzes has a Ph.D. in geology from Stanford University. He conducted postdoctoral research at Stanford and as a Mendenhall Fellow at the U.S. Geological Survey. His research explores the interaction of faulting, stress, and fluid flow. He is currently an assistant professor at Temple University and a visiting professor at the School for Renewable Energy Science.

STEPHEN P. BECKER ~ *Bureau of Economic Geology, Jackson School of Geosciences, University of Texas at Austin, Texas 78758*

Stephen P. Becker received his B.S. and M.S. degrees in geology from the University of Missouri-Rolla (now Missouri University of Science and Technology) in 2001 and 2005 and his Ph.D. in geochemistry from Virginia Tech in 2007. He currently holds a postdoctoral position at the Bureau of Economic Geology at the University of Texas at Austin, working on the application of fluid inclusions to understanding fracturing and fluid-flow histories.

ACKNOWLEDGEMENTS

Support through the U.S. Department of Energy-Chemical Sciences, Geosciences, and Biosciences Division; the Office of Basic Energy Sciences grants DE-FG03-94ER14462 and DE-FG01-06ER06-02; the John A. and Katherine G. Jackson Foundation; and the Geology Foundation at the University of Texas at Austin are thankfully acknowledged. We thank David Mucciarone at Stanford University for stable isotope analyses and Bob Bodnar at Virginia Tech for access to his laser Raman microprobe. We thank journal reviewers Jim Boles, Astrid Makowitz, and Russel Davies, and Bulletin Editor Gretchen Gillis for insightful comments. Publication was authorized by the director, Bureau of Economic Geology, University of Texas at Austin.

Copyright ©2009. The American Association of Petroleum Geologists. All rights reserved.

Manuscript received June 11, 2008; provisional acceptance August 18, 2008; revised manuscript received December 19, 2008; final acceptance February 18, 2009.

DOI:10.1306/02180908080

by shale entrainment. The Moab fault thus exemplifies the complex interaction of fault architecture and diagenetic sealing processes in controlling the hydraulic properties of faults in clastic sequences.

INTRODUCTION

The interaction of faults in sedimentary basins with basin- and reservoir-scale fluid flow has been shown to be complex, depending on a multitude of parameters that include lithologic juxtaposition, rheology of faulted units, fault structure and internal architecture, and fault-controlled diagenesis (Allan, 1989; Knipe et al., 1997; Aydin, 2000). Driven by the desire to predict the integrity of petroleum reservoirs, the sealing properties of faults have received significant attention in recent years. Previous studies have emphasized juxtaposition, the geometry of entrained shale units, and the function of clay minerals and fault-rock cataclasis in affecting the petrophysical properties of fault rocks (Lehner and Pilaar, 1997; Yielding et al., 1997; Doughty, 2003; Davatzes and Aydin, 2005; Eichhubl et al., 2005). Preferred conduit behavior of faults in hydrocarbon systems and related effects of fault-controlled diagenesis on fault–fluid–flow behavior have received less attention (O’Brien and Woods, 1995; Eichhubl and Boles, 2000a, b; Boles et al., 2004; Solum et al., 2005). As a result, fault-seal analyses in industry practice routinely assess the impact of faults on cross-fault flow but commonly fail to assess fault-parallel flow. From a reservoir perspective, fault-controlled diagenesis may lead to diagenetic fault seals that are dependent on reservoir chemical conditions and tectonic or overburden loading rate. Other studies have emphasized the seismic signature of fault-related diagenetic zones as fossil hydrocarbon migration pathways and reservoir spillways in trap integrity analysis (Gartrell et al., 2004; Ligtenberg, 2005).

This study was designed to assess the effects of fault segmentation and fault architecture on controlling focused flow and diagenesis along the Moab fault, a basin-scale normal fault in east-central Utah (Figure 1). The Moab fault is probably one of

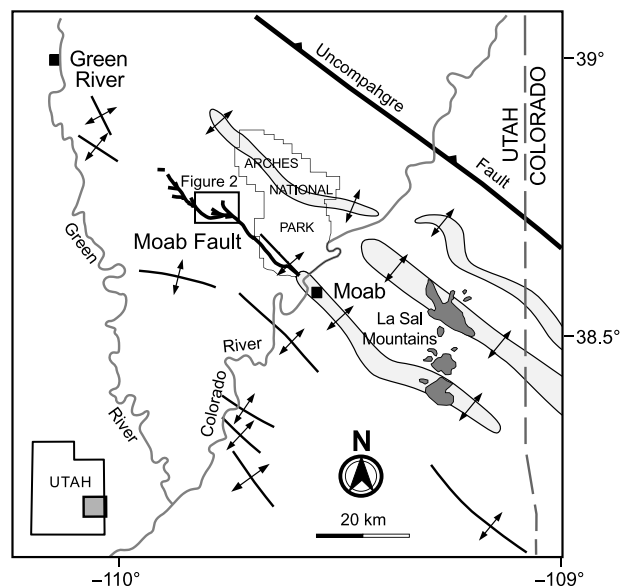


Figure 1. Location map of the Moab fault system in southern Utah (modified from Doelling, 1985). Salt anticlines are shaded gray.

the best studied surface-exposed normal fault systems in a clastic depositional setting (Foxford et al., 1996, 1998; Olig et al., 1996; Berg and Skar, 2005; Davatzes and Aydin, 2005; Davatzes et al., 2005; Fossen et al., 2005; Johansen et al., 2005; Solum et al., 2005). The 45-km-long (28-mi-long) fault displaces Pennsylvanian to Cretaceous units of the Paradox Basin by up to 960 m (3150 ft) of vertical stratigraphic offset (Doelling, 1988; Foxford et al., 1996, 1998). In the central section of the fault system around Courthouse Rock and Mill Canyon, the area of detailed investigation, the fault juxtaposes sandstones and siltstones of the Lower to Middle Jurassic Navajo, Entrada, and Curtis formations in the footwall against Upper Jurassic and Cretaceous shale and sandstone of the Morrison, Cedar Mountain, and Dakota formations in the hanging wall (Figure 2).

Prior studies by Foxford et al. (1996), Garden et al. (1997, 2001), and Chan et al. (2000) on diagenetic alteration processes along the Moab fault system described the spatial association of the fault with bleaching of hematite-cemented Jurassic eolian sandstone, as well as the occurrence of Fe and Mn oxides and carbonate cements in the vicinity of the fault. Based on isotopic analyses of hematite and calcite cements, fluid-inclusion analyses,

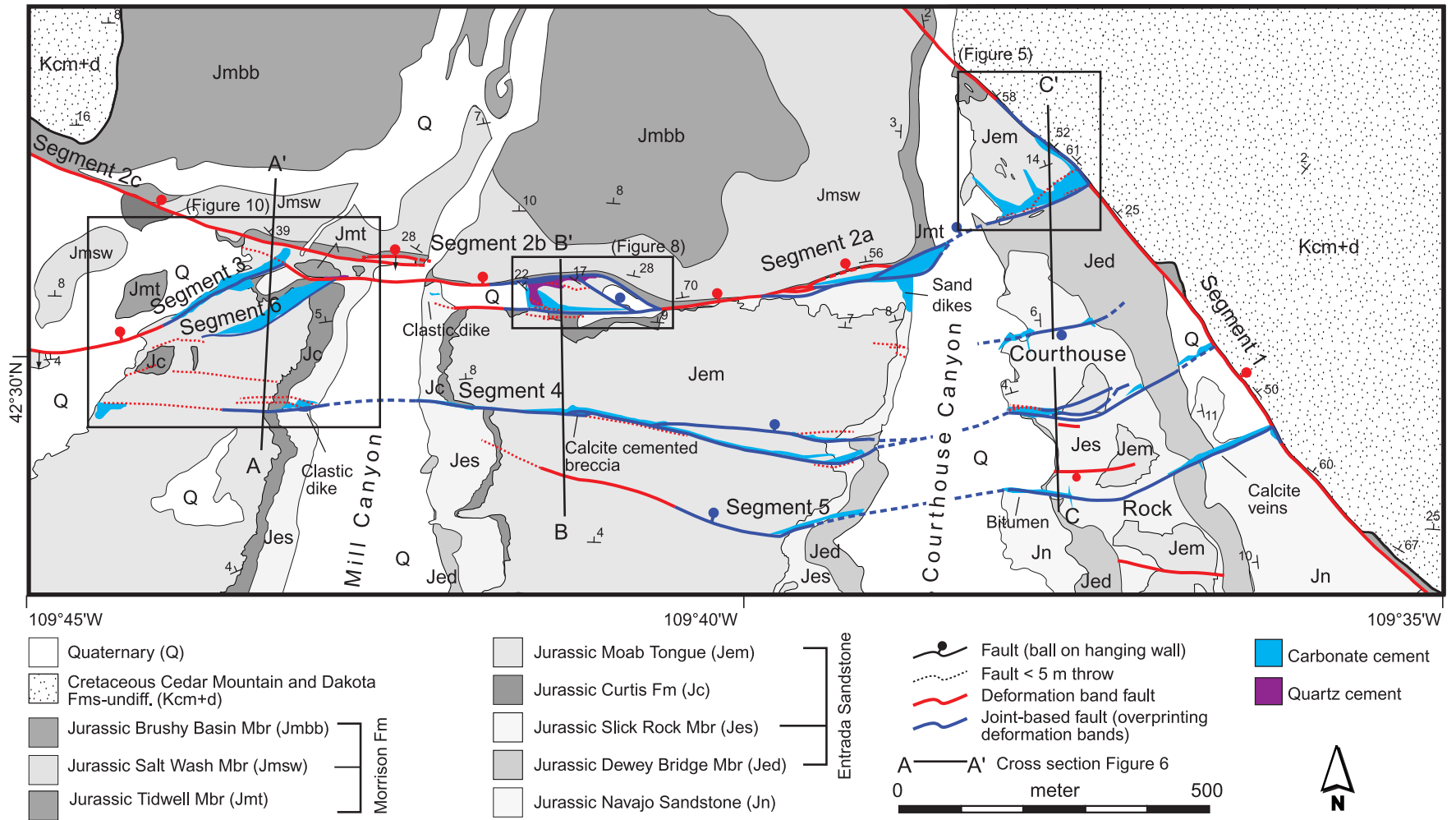


Figure 2. Geologic map of the Moab fault system in the Courthouse Rock–Mill Canyon area. Fault segments are numbered for reference in the text; segment 2 is further divided into three subsegments (2a, 2b, and 2c) by two right steps. The fault structure is from Davatzes et al., 2005.

and chemical modeling, Chan et al. (2000) concluded that upward-migrating, reduced brines mixed with meteoric water in the vicinity of the fault resulting in iron oxide remobilization and re-precipitation. Garden et al. (2001) provided an overview of fault-related diagenesis along the Moab fault emphasizing the southern section of the Moab fault at the entrance to Arches National Park. They attributed the bleaching of Jurassic sandstone units in the hanging wall of the Moab fault to the focused flow of hydrocarbons up along the fault and into the adjacent Moab anticline located in the hanging wall of the fault. Solum et al. (2005) described fault diagenetic changes in the clay gouge along the southern section of the fault system in the same locations.

This study focuses on the structural control of diagenetic alteration along the central section of the Moab fault around Courthouse Rock and Mill Canyon (Figures 1, 2). In contrast to the southern part of the Moab fault described by Garden et al. (2001), the central and northern parts are highly segmented into a series of curving and intersecting fault branches allowing a detailed assessment of the correlation of localized diagenetic alteration with the fault architecture and along-strike variation of fault–fluid–flow behavior. We mapped the distribution of fault-related diagenetic alteration as a proxy for paleofluid flow along segments of the Moab fault system based on the premise that the abundance and type of these alteration products reflect the focusing of fluid flow along the fault system and thus the permeability structure of the fault. Following a description of the structural elements and diagenetic alteration products observed along the fault system, we compare the distribution of diagenetic alteration products to the mapped distribution of deformation bands, joints, and sheared joints to establish controls of faulting processes on the hydraulic behavior of faults and conditions of paleofluid flow.

STRUCTURAL CHARACTERISTICS

The overall structure and internal architecture of the central section of the Moab fault system were

described in detail by Davatzes and Aydin (2003) and Davatzes et al. (2005). This area includes the intersection of the northwest-southeast–striking main segment 1 of the Moab fault with the curving and roughly east-west–striking segment 2, and the intersection of segment 2 with the curved segment 3 about 1 km (0.6 mi) farther west (Figure 2). The intersection of segments 1 and 2 at the mouth of Courthouse Rock has been referred to as Courthouse intersection. We will refer to the intersection of segments 2 and 3 west of Mill Canyon as Mill Canyon intersection. Two additional splays of the Moab fault, segments 4 and 5 in Figure 2, intersect segment 1 south of the Courthouse intersection; segment 6 branches off segment 2b. Segments 1–3 will be referred to as main segments, and segments 4–6 and smaller map-scale faults as subsidiary segments. Other regions of structural complexity along this section of the Moab fault system include two steps or fault relays along segment 2. Davatzes et al. (2005) characterized the relay east of Mill Canyon, separating segments 2a and 2b, as an extensional step. A contractional step west of Mill Canyon separates segments 2b and 2c. Although striations on slip surfaces indicate predominant dip-slip movement on the Moab fault system, Davatzes et al. (2005) attributed the extensional nature of the relay east of Mill Canyon to a right-lateral strike-slip component (rake of slip vector 80° east) resulting in fault-normal extension along the right-stepping array. Similarly, they attributed fault-normal contraction along the right-stepping array east of Mill Canyon to a left-lateral strike-slip component.

Segments of the Moab fault system that offset sandstones are composed of two classes of structural elements: (1) deformation bands and slip surfaces and (2) joints and sheared joints. Deformation bands are tabular zones of localized deformation in sandstones that accommodate shear by grain translation and rotation and typically involve grain fracture and porosity reduction (Antonellini and Aydin, 1994). Some segments of the Moab fault system are composed of zones of multiple narrowly spaced subparallel deformation bands, with most slip concentrated along associated, discrete slip surfaces (Figure 3a). Joints are discrete

discontinuities or fractures forming in opening mode that can be reactivated in shear, resulting in the formation of multiple generations of splay fractures (Pollard and Aydin, 1988). Such joint-splay fracture systems can coalesce into breccia zones and through-going fault surfaces (Davatzes et al., 2003, 2005; Myers and Aydin, 2004).

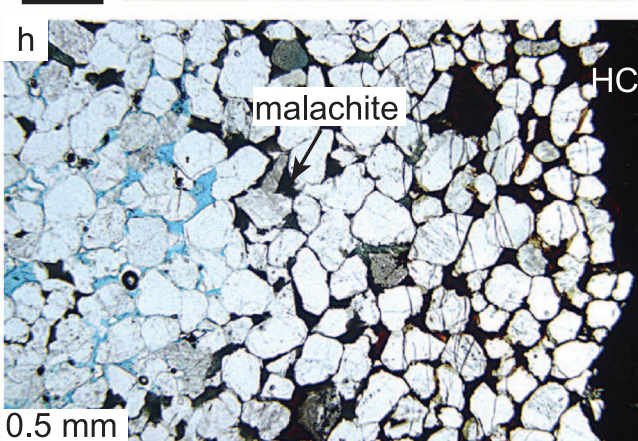
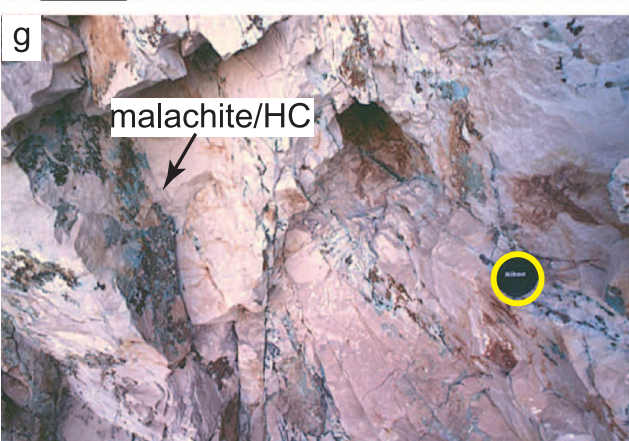
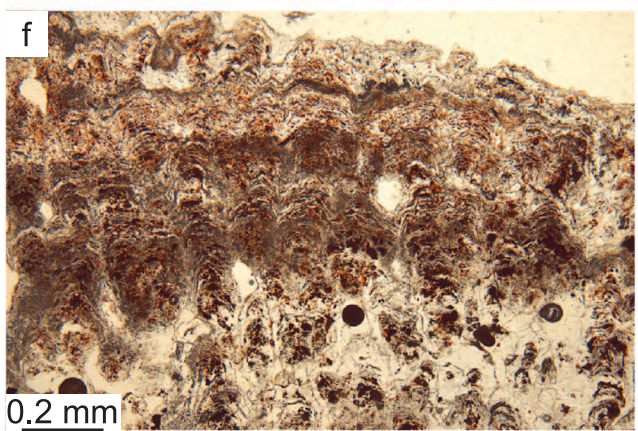
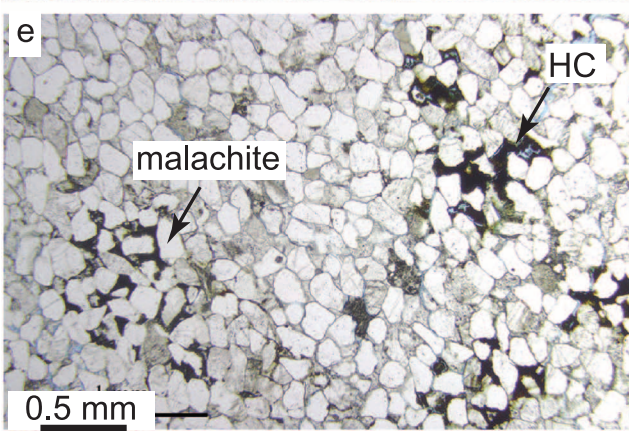
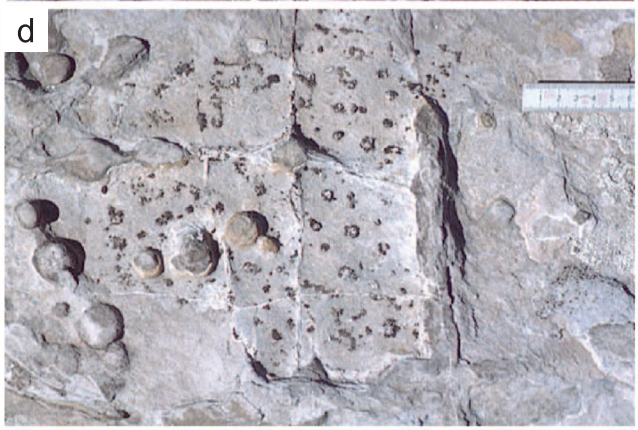
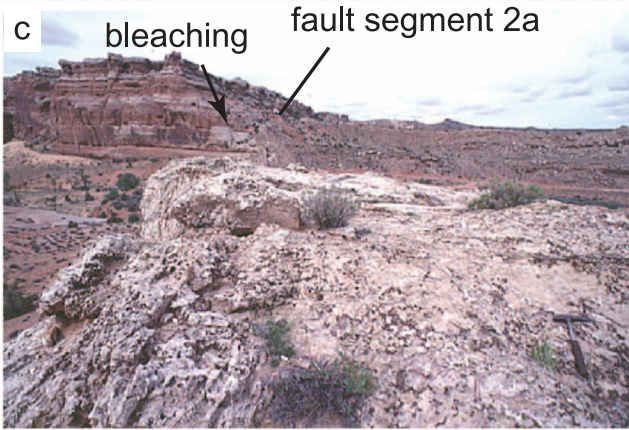
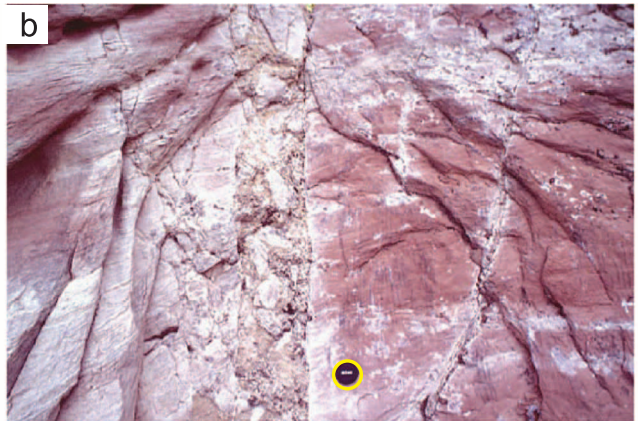
The distribution of deformation bands and joints along fault segments of the Moab fault system is controlled by fault geometry and the extensional or contractional character of fault segments. In general, joints and sheared joints are dominant in the fault core and fault damage zone in areas of structural complexity that promote extension such as fault intersections and releasing steps or bends, whereas planar fault segments and restraining steps or bends are dominated by deformation bands and slip surfaces. For fault segments that contain both deformation bands and (sheared) joints, the formation of deformation bands generally precedes the formation and shearing of joints. In areas of structural complexity that promote extension such as releasing fault bends and fault intersections, deformation-band faults are overprinted by joints, sheared joints, and breccias. South of the Courthouse Rock intersection, segment 1 is composed of deformation bands and zones of deformation bands without joints or sheared joints (Figure 2). In contrast, segment 1 north of the Courthouse Rock intersection and segment 2a are composed of deformation bands overprinted by an extensive network of joints and breccias in the vicinity of the intersection (Figure 2).

Clastic dikes are spatially and texturally distinct from fault breccias (Foxford et al., 1996). One is observed on the east wall of Mill Canyon at the western tip of fault segment 2a (Figures 2, 3b) hosted in the partially bleached sandstone of the Slick Rock Member of the Entrada Sandstone. This dike is 10–30 cm (4–12 in.) in width and contains angular pieces of sandstone of up to 30 cm (12 in.) in size in a sandy calcite-cemented matrix. Another clastic dike is observed on the west wall of Mill Canyon along fault segment 4 (Figure 2). At both locations, fragments of lithified sandstone appear to be derived from the adjacent host sandstone.

Previous studies have shown that most deformation bands are less permeable than the undeformed sandstone thus acting as barriers or baffles to fluid flow (Antonellini and Aydin, 1994; Fowles and Burley, 1994; Main et al., 2000). Joints are opening-mode fractures that tend to act as preferred flow conduits unless sealed by mineral precipitation. Small amounts of slip along sheared joints increase joint connectivity by the formation of splay fractures. Larger amounts of shearing lead to cataclasis that tends to reduce permeability along and across sheared joints (Flodin et al., 2004; Myers and Aydin, 2004). Because of the different hydraulic properties of these structural elements, we hypothesize that the permeability structure of a fault system is, to first approximation, controlled by the distribution and overprinting relationships of the structural elements. We mapped the distribution of diagenetic alteration products as a proxy for paleofluid flow in an effort to test this hypothesis.

DIAGENETIC ALTERATION PRODUCTS

The map-scale diagenetic alteration adjacent to the Moab fault in the Courthouse Rock–Mill Canyon area affects primarily the Jurassic eolian sandstone units of the Navajo Sandstone, Entrada Sandstone, and Curtis Formation (Figure 2). In the Courthouse area, the Curtis Formation separates the underlying Slick Rock Member from the overlying Moab Tongue member of the Entrada Sandstone. A detailed stratigraphic and lithologic description of these units was given by Doelling (1988, 2003), Foxford et al. (1996), and Chan et al. (2000). The Navajo Sandstone is a fine-grained eolian quartz arenite to subarkose sandstone. The sandstones of the Slick Rock and Moab Tongue members of the Entrada Sandstone and of the Curtis Formation are fine- to medium-grained quartz arenites. These sandstone units alternate with siltstone and silty sandstone of the Dewey Bridge Member at the base of the Entrada Sandstone, and with mudstone of the Curtis Formation. The Moab Tongue member of the Entrada Sandstone is overlain by sandstone and shale units of the Morrison and Cedar Mountain formations.



In the Courthouse Rock–Mill Canyon area, the following products of diagenetic alteration are observed.

Carbonate

Fault-related carbonate cement occurs as calcite, ferroan dolomite, and malachite. Calcite cement is the most abundant fault-related cement found along the Moab fault in the Courthouse Rock–Mill Canyon area. Calcite cementation occurs in two forms: (1) as spherical calcite concretions and (2) as calcite veins and associated cement halos (Figure 3c, d). Calcite concretions are up to 5 cm (1.9 in.) in diameter, typically decreasing in diameter with distance away from faults. Locally, concretions are dense enough to coalesce and to form cemented layers. In thin section, concretionary calcite forms poikilotopic pore cement (Figure 3e) completely filling the pore space with the exception of pockets of residual hydrocarbons and micritic malachite. Calcite veins are up to 4 cm (1.5 in.) thick and are in most cases surrounded by a 2–3-cm-thick (0.7–1.1-in.-thick) halo of pore-filling calcite cement. Unlike fracture skins described elsewhere that mantle otherwise uncemented fractures (Robinson et al., 1998), these cement halos only occur where the fracture is cemented and are in optical continuity with the fracture-filling cement. Calcite cement fills the entire aperture of fractures but is frequently discontinuous along the length of fractures. Fractures adjacent to cemented fractures and of same orientation may remain uncemented. Lack of consistent crosscutting relations among cemented, partially cemented, and

uncemented fractures indicates that the partial cement fill of fractures reflects selective cementation of an existing fracture system instead of fracture formation outlasting fracture cementation. We found no evidence that calcite cement precipitation preceded fracture formation. In addition to concretions, veins, and halos along veins, calcite occurs as diffuse pore-filling cement in sandstone adjacent to the main segments of the Moab fault system.

Some calcite veins are characterized by a brown outcrop color that is noticeably more common along the main fault segments. In thin section, brown calcite contains abundant brown to orange organic inclusions. In one sample of brown calcite cement from fault segment 2a at Courthouse Rock, these organic inclusions form rugose laminae akin to microbial mats (Figure 3f). Some calcite veins contain rhombs of early ferroan dolomite cement as determined by energy dispersive spectroscopy. These rhombs line the fracture walls and are followed by later Fe-poor calcite.

Micritic malachite is found as late-stage pore-filling cement in contact with hydrocarbons (Figure 3g, h). The textural similarity of pockets of pore-filling micritic malachite enclosed in poikilotopic calcite with similarly occurring residual hydrocarbon (Figure 3e) suggests that micritic malachite replaces hydrocarbons. Where malachite is observed with calcite and quartz cement, malachite is the most recent cement phase.

Oxides

The eolian Lower to Middle Jurassic sandstones are typically characterized by a uniform red color

Figure 3. (a) Zone of deformation bands along the main trace of fault segment 1. The fault slip is mostly concentrated on the slip surface bounding the zone toward the viewer (surface behind pen). (b) Clastic dike in the Slick Rock Member of the Entrada Sandstone on the east side of Mill Canyon. See Figure 2 for the location. Lens cap (5 cm [1.9 in.]) for scale (circled). (c) Calcite cementation in the sandstone of the Moab Tongue member of the Entrada Sandstone at the Courthouse fault intersection (segment 2a). Calcite cement forms concretions and veins with associated cement halos. The Slick Rock sandstone in the footwall adjacent to the fault is bleached (background). (d) Calcite concretions and veins in the Moab Tongue sandstone. Veins are typically associated with halos of pore-filling cement. Note the discontinuous nature of vein cement and cement halo. Scale in centimeter. (e) Sandstone of the Moab Tongue member cemented by poikilotopic calcite in a calcite concretion at Courthouse Rock. Hydrocarbon (HC) fills remnant pore space. Some hydrocarbons are replaced by micritic malachite. (f) Microbial mats in vein calcite within the Cedar Mountain Formation 120 m (394 ft) northwest of the Courthouse intersection. (g) Malachite and hydrocarbon (HC) in joints of quartz-cemented Moab Tongue, Mill Canyon extensional step, adjacent to segment 2b. Lens cap (5 cm [1.9 in.]) for scale (circled). (h) Micritic malachite at the outer margin of HC filling joint and adjacent pore space.

that results from thin grain coats of hematite. This type of hematite cement is considered the result of early diagenesis in a continental depositional setting (Walker, 1975; Shawe, 1976; Walker et al., 1978; Turner, 1980; Chan et al., 2000; Eichhubl et al., 2004). Adjacent to faults and preferentially in coarser grained sandstone units, these reddish sandstones are frequently bleached (Foxford et al., 1996; Garden et al., 1997, 2001). Sandstones of the Moab Tongue member of the Entrada Sandstone and Navajo Sandstone are bleached throughout the Courthouse Rock–Mill Canyon area. Less porous and more cemented sandstones of the Slick Rock Member of the Entrada Sandstone are bleached over distances of up to 50 m (164 ft) away from the Moab fault (Figure 3c). Bleaching of fine-grained sandstone and siltstone of the Dewey Bridge Member of the Entrada Sandstone extends typically only 1–2 cm (0.3–0.7 in.) away from joints and faults (Figure 4a). The Fe and Mn oxides are locally reprecipitated in the wider Moab fault area as concretions and pipes as described in detail by Chan et al. (2000) from an area about 20 km (12 mi) west of Courthouse Rock. Liesegang bands of iron oxides were observed at Courthouse Rock around open sections of joints that are partially cemented by calcite, indicating that Liesegang band formation postdated calcite cementation (Figure 4b).

Quartz

The Lower to Middle Jurassic sandstones generally contain moderate amounts of quartz overgrowth cement, with the exception of the 1–2-m-thick (3–6-ft-thick) top layer of the Slick Rock Member of the Entrada Sandstone. The higher quartz cement content of the Slick Rock sandstone appears to be regional in extent and thus not fault controlled. The abundance of quartz overgrowth cement increases in the Moab Tongue sandstone adjacent to the Mill Canyon extensional step (Figures 2, 4c). We have not observed microcrystalline quartz or chalcedony cement that is spatially related to the Moab fault system. Chert cement described by Haszeldine et al. (2005) appears spatially associated with the hinge of the Moab anticline instead of the Moab fault.

Barite

Minor amounts of pore-filling poikilotopic barite were observed in a sample of Moab Tongue adjacent to the Moab fault. Extensive occurrence of barite was described by Morrison and Parry (1986) and Breit et al. (1990) from faults southeast of Moab. Based on the sulfur isotopic composition of barite found in the Upper Jurassic Morrison Formation, Breit et al. (1990) attributed barite formation to fluids originating in the underlying Pennsylvanian evaporites.

Hydrocarbons

Residual hydrocarbons are observed along joints (Figures 3h, 4a) and in sandstone pores where they are typically encased in calcite cement (Figure 3e).

DISTRIBUTION OF DIAGENETIC ALTERATION PRODUCTS

Courthouse Intersection

At Courthouse Rock, segments 1 and 2a of the Moab fault system intersect at approximately 70° (Figures 2, 5). The fault core of segments 1 and 2a is composed of deformation bands that are overprinted by calcite-cemented joints and fault breccia (Figures 4d, 5a). Within the triangular fault block formed by this acute fault intersection angle, bleached sandstone of the Moab Tongue member of the Entrada Sandstone is locally cemented with concretionary calcite and vein calcite (Figure 3c, d) and malachite (Figures 3e, 5). This cement is more abundant in the damage zone adjacent to the fault intersection and along segment 2a but distinctly less abundant adjacent to fault segment 1. The localization of calcite in the fault block along fault segment 2a reflects the abundance of joints as mapped by Davatzes et al. (2005) (Figure 5b). No clear correlation is observed between the outcrop-scale distribution of calcite cement and deformation bands (Figure 5c). Brown organic-rich calcite is found as diffuse cement in the footwall of segment 1 and as a 20–30-cm-thick (9–12-in.-thick)

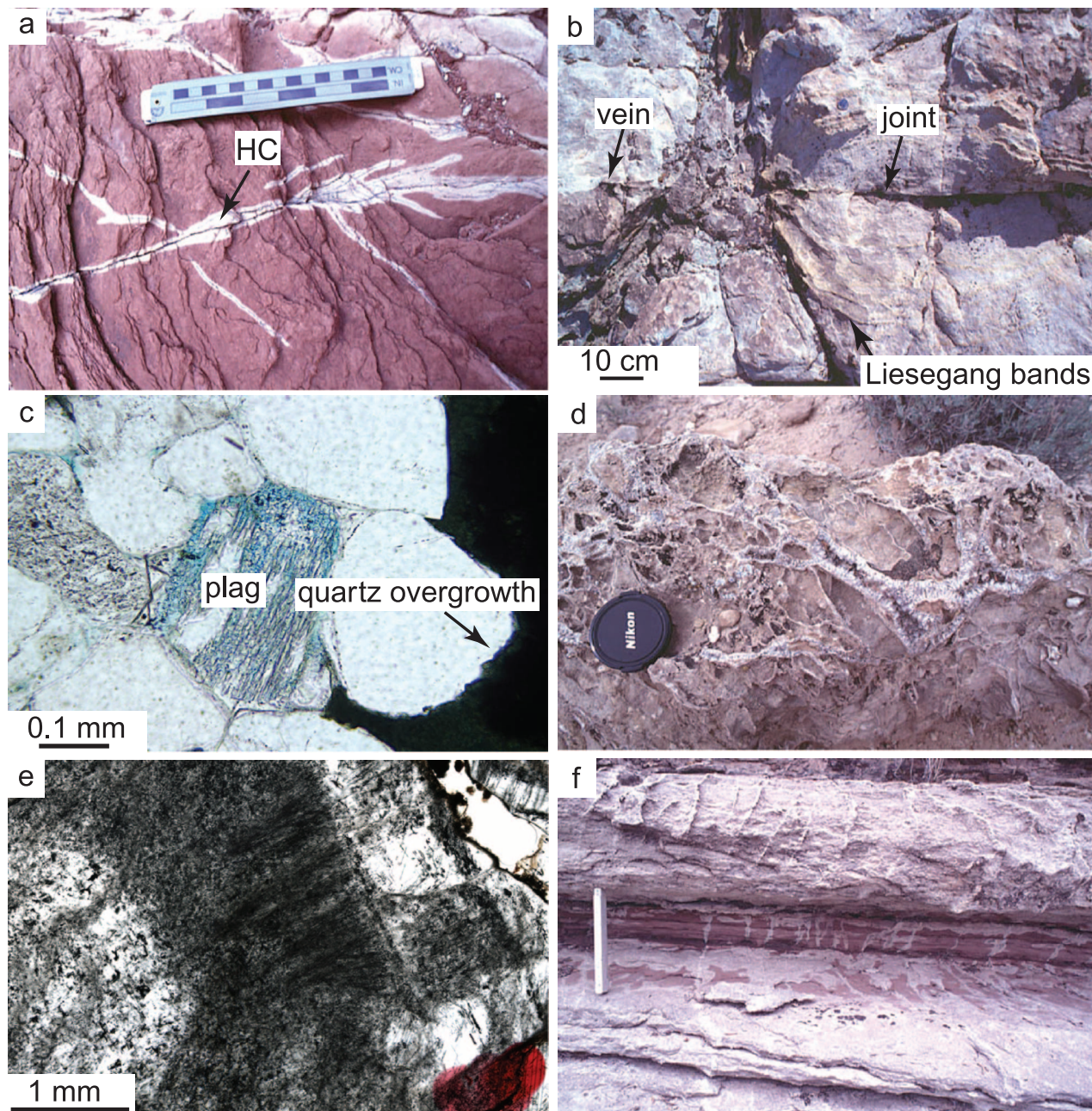


Figure 4. (a) Bleached siltstone of the Dewey Bridge Member adjacent to hydrocarbon (HC)-stained joints. (b) Incomplete cementation of joints by calcite vein cement renders joints as open fluid-flow conduits as evidenced by Liesegang bands centered on the uncemented section of the joint. Moab Tongue sandstone at the Courthouse fault intersection. (c) Quartz and feldspar (plag) overgrowth cement in the Moab Tongue sandstone, Mill Canyon step. Plagioclase is mostly dissolved after overgrowth formation. (d) Fault breccia cemented by calcite vein fill from fault segment 5. (e) Calcite with growth zones of varying density of primary fluid inclusions. Growth from left to right. Sample from the location in panel d. (f) Joints with associated bleaching halos in red siltstone of the Curtis Formation continue as calcite-cemented veins into the overlying Moab Tongue sandstone. Mill Canyon intersection. Scale is 22 cm (9 in.).

cemented layer along the fault surface of segment 2a (Figure 5a). Malachite occurs as pore-filling cement and is most abundant in the vicinity of the fault-segment intersection.

In cross section, calcite cement is concentrated within the top 5 m (16 ft) of the Moab Tongue sandstone northwest of the fault intersection (Figure 6, section CC'). With the sandstone dipping 10–15°

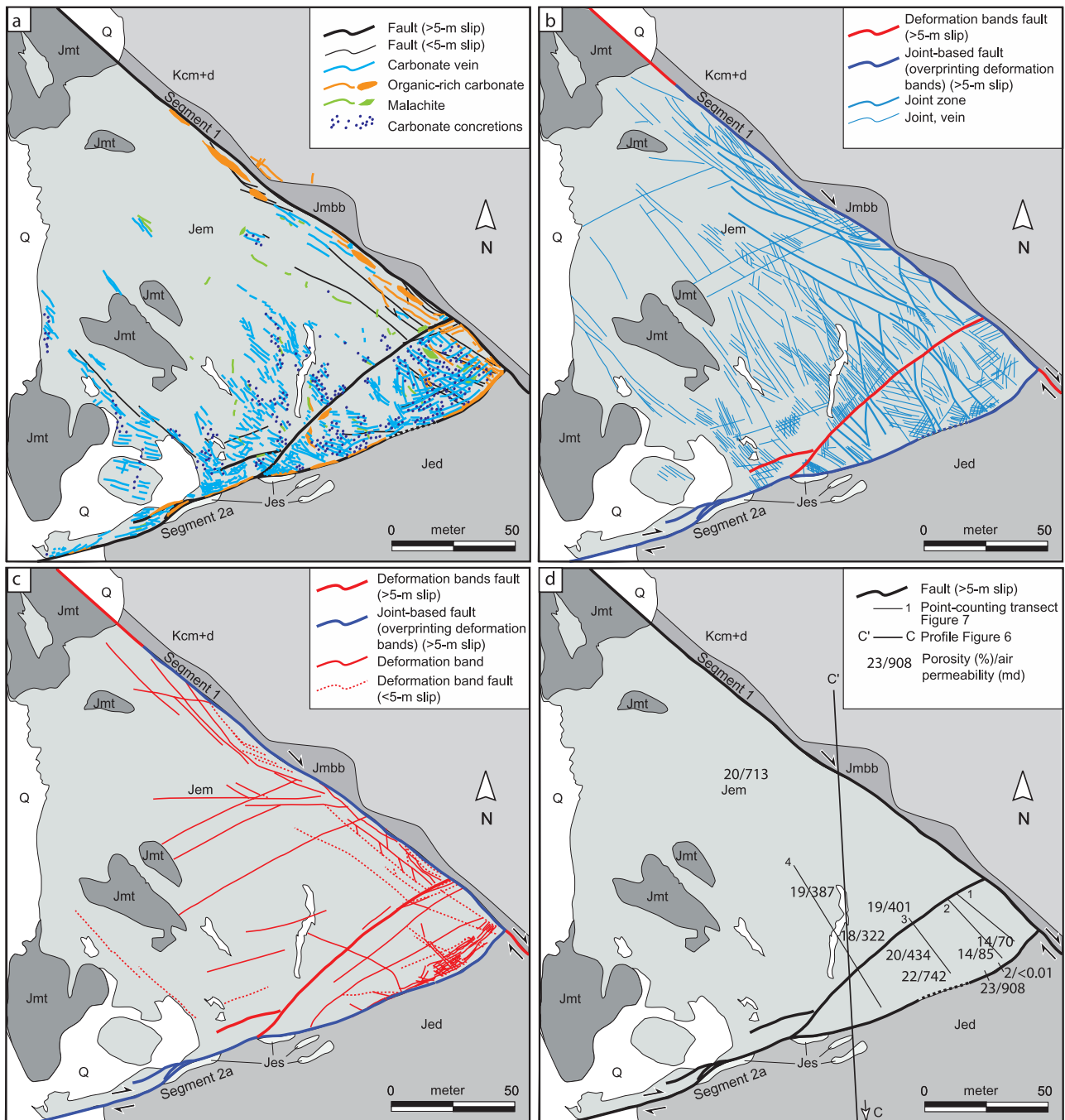


Figure 5. (a) Cement distribution map of the Courthouse fault intersection. See Figure 2 for the legend to the stratigraphic units. (b) Distribution of joint zones and joints. (c) Distribution of deformation bands. (d) Helium porosity and air permeability measurements, and location of cross section (Figure 6) and point-counting transects (Figure 7).

away from the fault intersection, the highest cement abundance thus coincides with the structural high of the fault block. Although eroded away at the fault intersection, overlying siltstone and shale of the Jurassic Tidwell Member of the Morrison Formation are preserved 100 m (328 ft) west to the

intersection (Jmt in Figure 5), indicating that the cemented horizon corresponds stratigraphically to the uppermost part of the Moab Tongue member, immediately below the eroded siltstone and shale.

The abundance of calcite concretions and of veins and their associated cement halos was quantified

South

North

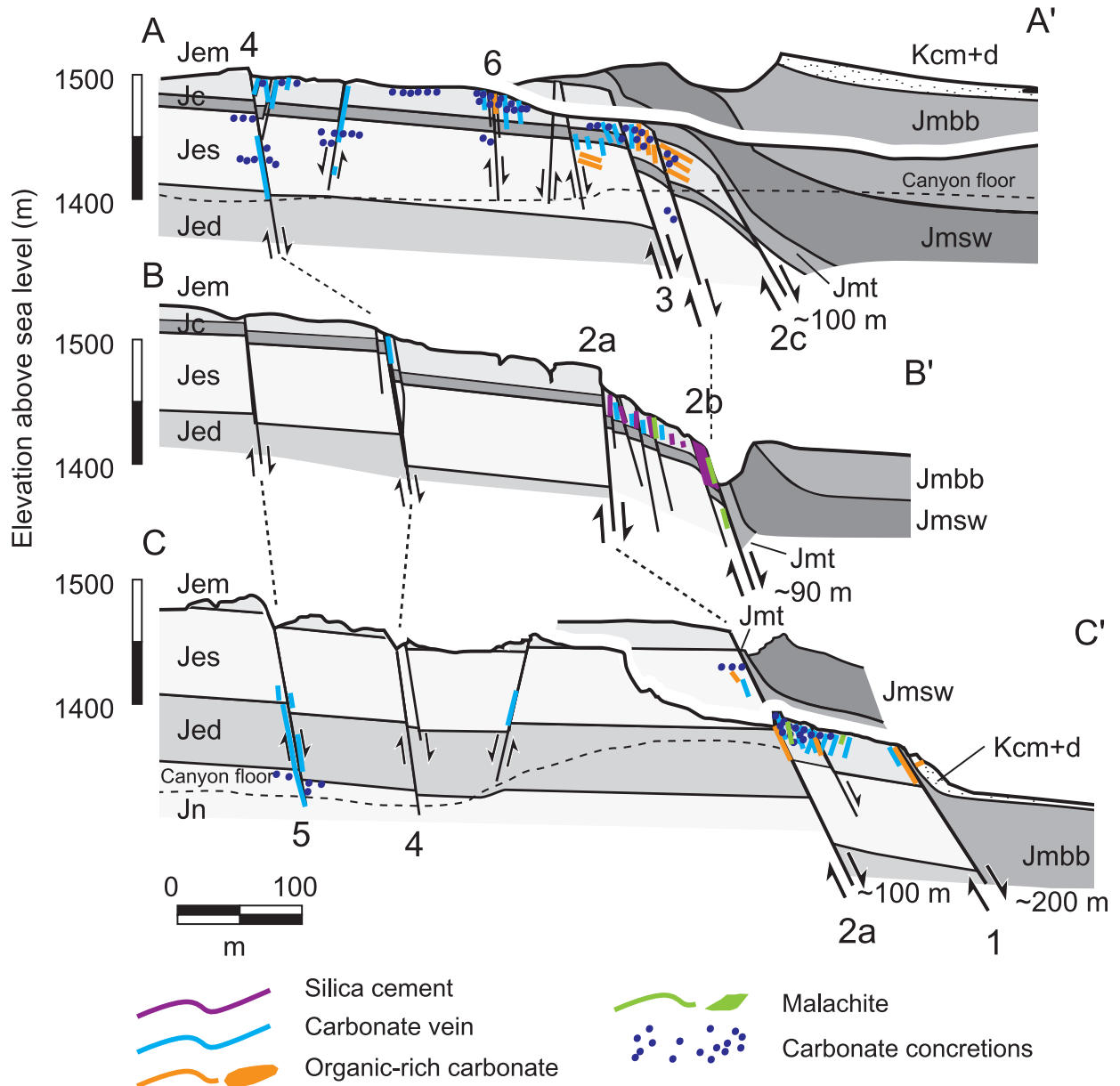


Figure 6. Cross sections across the Moab fault system in the Courthouse Rock–Mill Canyon area showing the distribution of diagenetic alteration products in relation to the fault structure. Numbers refer to fault segments as shown in Figure 2. Estimates of fault throw are indicated in meters. See Figure 2 for the section locations and the legend to stratigraphic units.

along four outcrop-scale points counting traverses striking roughly perpendicular away from fault segment 2a. (Figure 5d). Outcrop point counting was performed by overlying a square grid of 1-m (3-ft) side length with 100 grid points over the outcrop surface at regular intervals along the transect lines. Whereas concretions host more calcite compared to veins adjacent to fault segment 2a

(Figure 7a), veins extend farther away from the fault (Figure 7b). In thin section, concretions were found to contain about 20% of calcite as poikilotopic pore-filling cement completely filling the intergranular volume of 20%. Veins contain 100% carbonate but are typically less than 1 mm in thickness whereas cement halos are 1–3 cm (0.3–1.1 in.) thick. Similar to concretions, cement halos contain

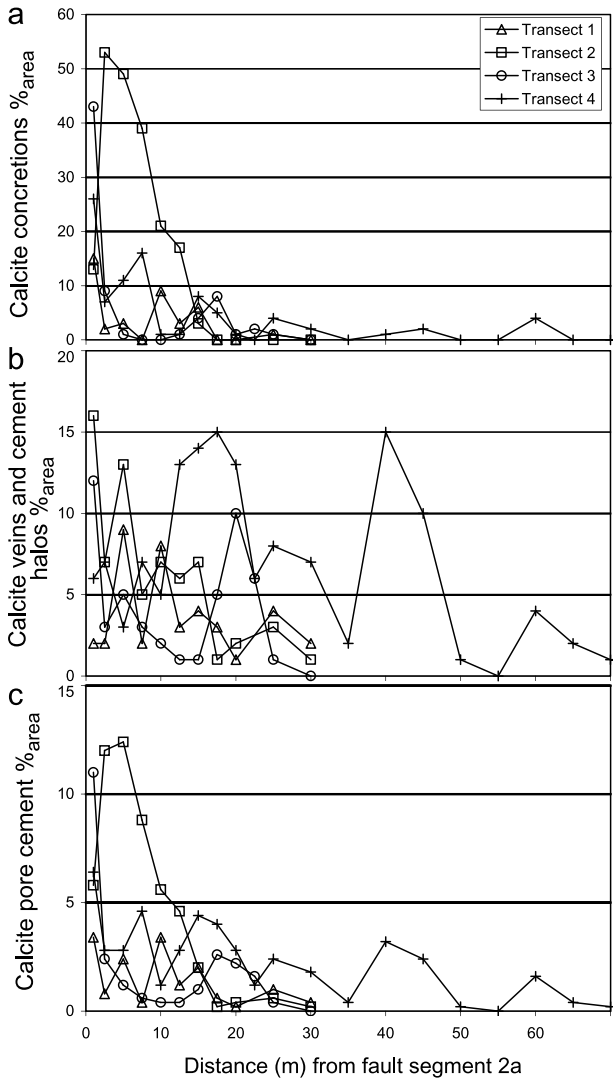


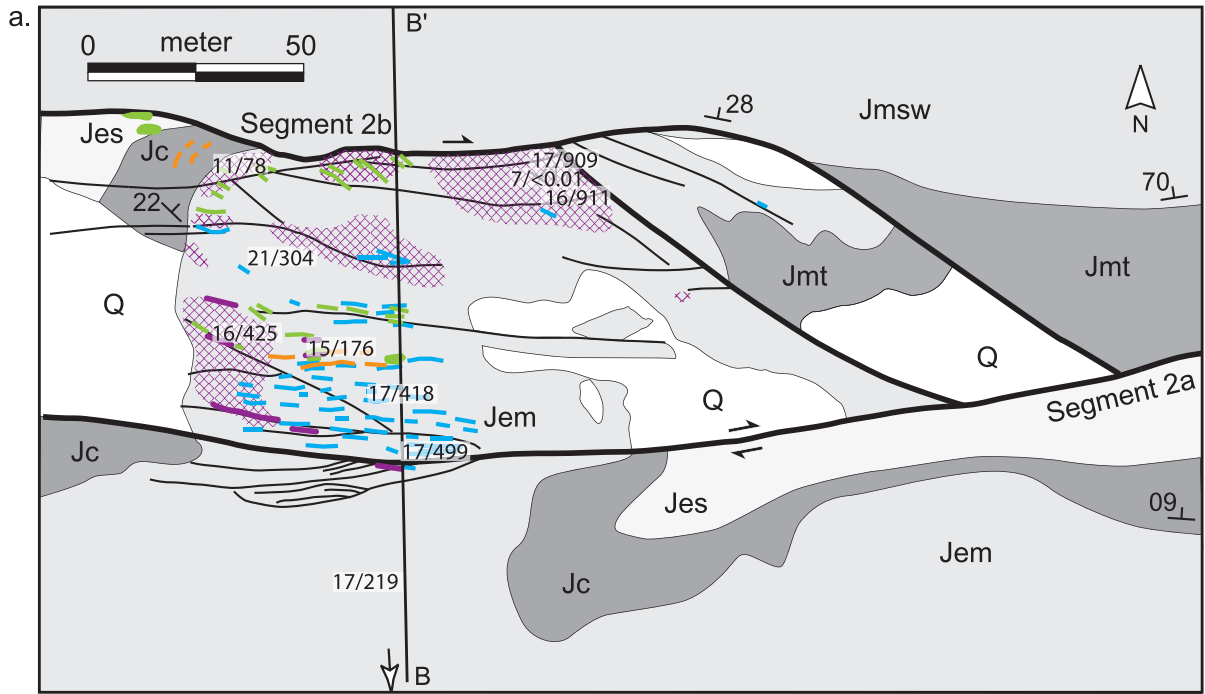
Figure 7. Outcrop point-counting transects across Moab Tongue sandstone at the Courthouse fault intersection. (a) Concretions; (b) veins; (c) calcite cement contained in concretions and veins for a 20% abundance of pore-filling calcite cement as measured by petrographic point counting. See Figure 5d for the transect locations.

about 20% calcite pore cement and thus represent the bulk of calcite associated with veins. The combined calcite content of concretions and veins as a function of distance from the fault is shown in Figure 7c. The total volume of calcite cement in the Moab Tongue sandstone at the Courthouse branch point is estimated by integrating the amount of calcite over the transect lengths and by multiplying by the thickness of the cemented layer and by the length of the cemented area.

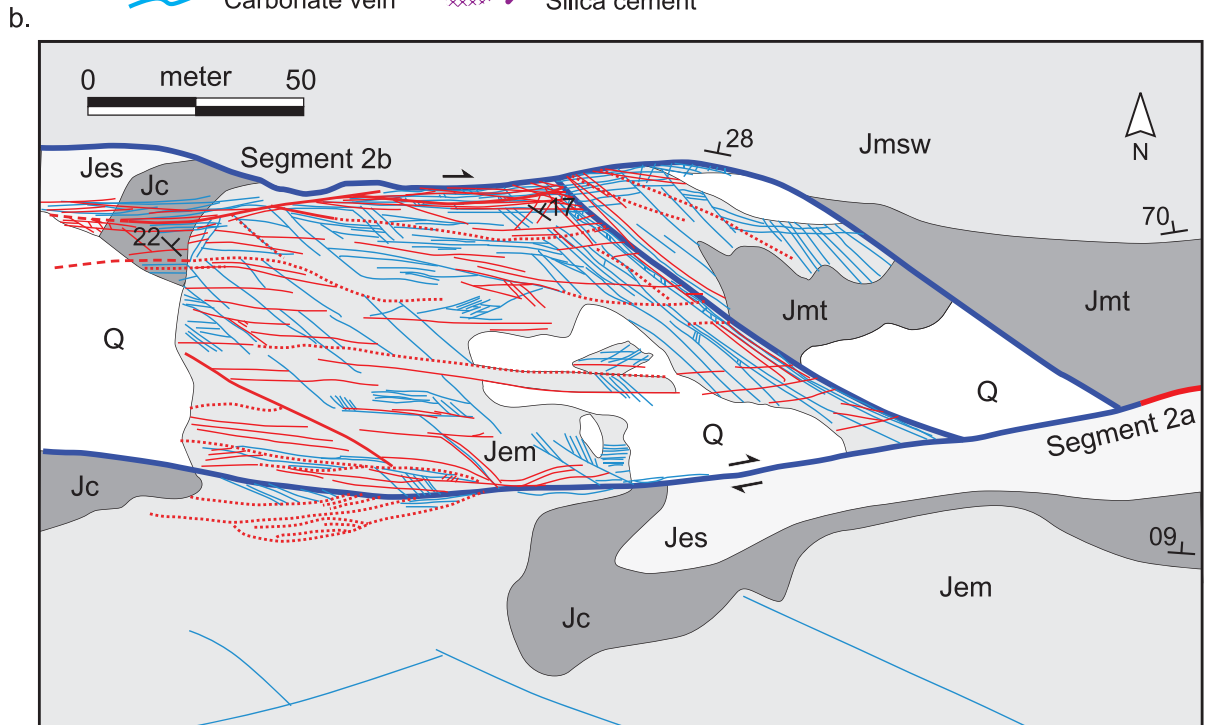
The thickness of the cemented layer is taken here as 5 m (16 ft), the approximate thickness of the Moab Tongue member in the Courthouse Rock area. The length of the cemented area, measured perpendicular to the transects, is approximately 100 m (328 ft). Thus, based on an average calcite content of 4% more than 40 m (131 ft) of transect distance, the total amount of calcite at this location is about 800 m³ (28,252 ft³). In a following section, we use this estimate to calculate a minimum volume of fluid required for calcite precipitation in this area.

Mill Canyon Extensional Step

About 300 m (984 ft) east of Mill Canyon, segment 2a of the Moab fault system steps to the right by about 80 m (262 ft) and continues west into Mill Canyon as segment 2b (Figures 2, 8a). Sandstone of the Moab Tongue member between segments 2a and 2b is characterized by locally increased abundance of quartz overgrowth cement (Figures 4c, 8a). Quartz-cemented Moab Tongue sandstone is distinctly less friable and mapped in the field based on the sharper sound when tapped with a rock hammer compared to lesser cemented sandstone away from the step. Enhanced quartz overgrowth cement within the step appears to correlate with areas of high joint density (Figure 8b). Abundance of quartz overgrowth cement was determined by petrographic point counting of eight samples collected along a transect across the extensional fault step. Point counting was performed on thin sections stained for K-spar of samples devoid of cataclasis and impregnated with blue epoxy, with 600 counts per thin section. Abundance of quartz overgrowth cement increases from less than 6% away from the fault step to about 11% along fault segment 2b (Figure 9). Calcite and malachite occur as fracture-filling cement and as pore cement adjacent to fractures. Malachite is most abundant along hydrocarbon-stained joints (Figure 3g, h) in quartz-cemented sandstone adjacent to fault segment 2b. Calcite concretions are noticeably absent in the Mill Canyon extensional step. Fractures containing calcite and malachite cement crosscut quartz overgrowth cement. Calcite and malachite



- Fault >5-m slip
- Fault <5-m slip
- Carbonate vein
- Organic-rich carbonate
- Malachite
- Silica cement
- 23/908 Porosity (%) / air permeability (md)



- Deformation band fault (>5-m slip)
- Joint-based fault (overprinting deformation bands) (>5-m slip)
- Deformation band fault (<5-m slip)
- Deformation band
- Joint, vein

Figure 8. (a) Cement distribution, helium porosity and air permeability measurements, and location of cross section (Figure 6) for the Mill Canyon extensional step. (b) Structure map. See Figure 2 for the legend to the stratigraphic units.

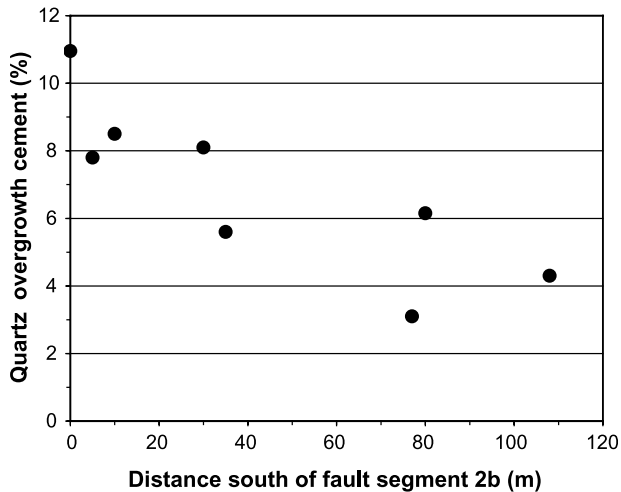


Figure 9. Abundance of quartz overgrowth cement in Moab Tongue sandstone as a function of distance away from segment 2b in the Mill Canyon extensional step. Quartz cement abundance was determined by petrographic point counting.

fracture cement thus postdates quartz overgrowth cementation.

Mill Canyon Intersection

West of Mill Canyon, calcite occurs in two distinct structural positions. Similar to the Courthouse intersection, calcite concretions and veins occur in the vicinity of fault intersections within triangular fault blocks of intersecting fault segments (Figure 10a). One such fault block is formed by segments 2b and a segment, referred to as segment 6, which branches off segment 2b and terminates about 2 km (1.2 mi) to the southwest (Figure 10a). A second triangular fault block is formed by segments 2b and 3. Segment 3 continues southwest as the main branch of the Moab fault system. At both fault intersections, the Moab Tongue sandstone and, to a lesser extent, the underlying Curtis Formation and Slick Rock Member of the Entrada Sandstone are cemented with calcite concretions and veins.

The contractional step between segments 2b and 2c is structurally characterized by abundant deformation bands parallel to the fault segments (Figure 10b). Joints and calcite-cemented veins are absent except for the vicinity of the intersection of segments 2b and 3 where organic-rich calcite veins are aligned parallel, and along strike, of the abutting segment 3 (Figure 10a).

Other Occurrences of Fault-Related Cementation

In addition to these areas of fault-related calcite and quartz cementation, calcite vein cement occurs along fault segment 4. This fault segment branches off segment 1 southeast of the Courthouse intersection (Figure 2) and can be traced across Courthouse Canyon and Mill Canyon for about 400 m (1312 ft) west of Mill Canyon where it terminates (Figure 10b). Calcite cementation is found in the west wall of Mill Canyon (Figure 10a), between Mill and Courthouse canyons, and in the west wall of Courthouse Rock (Figure 2). At all three locations along segment 4, calcite veins are spatially associated with bleaching and traces of hydrocarbons. The western termination of segment 4 is notable for the association of veins and concretions with joints located in an extensional quadrant southwest of the tip, extending 40 m (131 ft) from the fault tip (Figure 10a). Segment 5 also shows extensive calcite vein cement and some concretions, bleaching in both east and west faces of Courthouse Rock, and where segment 5 abuts against segment 1 (Figures 2, 4d). At all of these locations, calcite forms thick veins or stockworks where joint density is high but only little pore-filling cement as concretions or cement halos.

STABLE ISOTOPIC AND FLUID-INCLUSION CHARACTERIZATION OF FAULT-RELATED CEMENT

Methods

Stable isotope analyses of calcite vein and fault cement and concretions were performed at the Stanford Stable Isotope Biochemistry Laboratory on a Thermo Finnigan Kiel III Carbonate Device. Powdered samples were obtained using a dental drill or by crushing mechanically separated vein cement fragments.

Permanently mounted doubly polished thin sections of fault-related cements approximately 50–60 μm in thickness were prepared for fluid inclusion analysis. Thin sections were broken into smaller

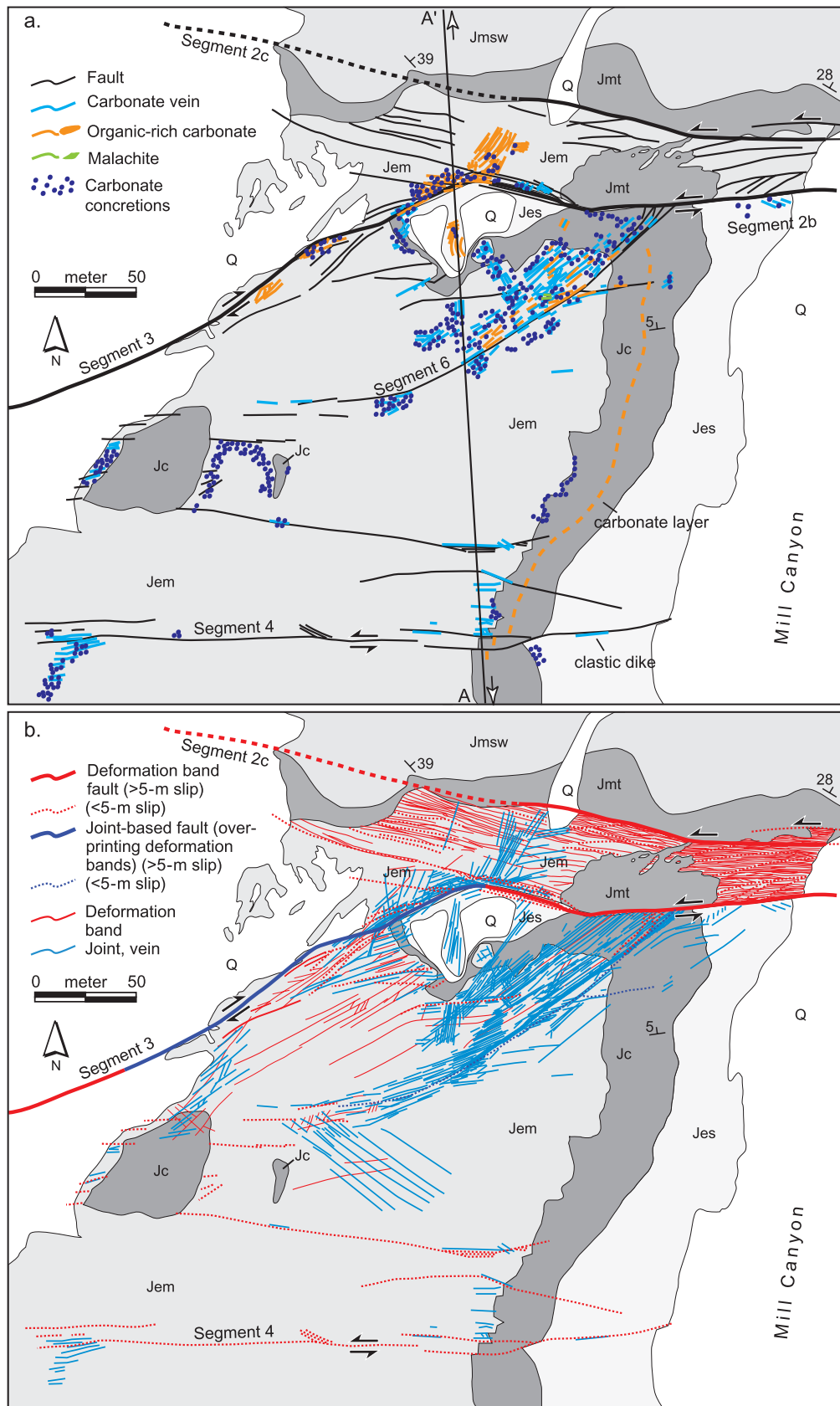


Figure 10. (a) Cement distribution, helium porosity and air permeability measurements, and location of cross section (Figure 6) for the Mill Canyon fault intersection area. (b) Structure map. See Figure 2 for the legend to the stratigraphic units.

fragments and placed into a USGS-type gas-flow heating and freezing stage mounted on an Olympus BX51 microscope equipped with a 40× objective (numerical aperture [N.A.] = 0.55) with 10× oculars. The stage was calibrated at 374.1 and 0.0°C using synthetic pure H₂O fluid inclusions and at -56.6°C using synthetic CO₂ fluid inclusions. The liquid-vapor homogenization temperature (T_h) and final ice melting temperature (T_m) of individual inclusions within fluid-inclusion assemblages were determined to ±0.5 and ±0.1°C, respectively, using thermal cycling intervals of 1 and 0.2°C. Raman spectroscopy was performed on several calcite-hosted fluid inclusions to check for the presence of CO₂ and CH₄ at the Vibrational Spectroscopy Laboratory in the Department of Geosciences at Virginia Tech using a JY Horiba LabRam HR (800 mm [31 in.]) spectrometer, with a 2400 grooves/mm grating and a slit width of 400 μm. The confocal aperture was set at 400 μm. Excitation was provided by a 514.53-nm Laser Physics 100S-514 Ar⁺ laser. The laser output was 50 mW at the source and less than 10 mW at the sample. The detector was an electronically cooled open-electrode CCD (charge-coupled device).

Results

The stable isotopic composition of calcite is shown in Figure 11a, which combines our own analyses with those by Chan et al. (2000) from the Courthouse Rock area and by Garden et al. (2001) from the southern part of the Moab fault system. The $\delta^{13}\text{C}$ values range between 0 and -15‰ PeeDee belemnite (PDB), and $\delta^{18}\text{O}$ values between -10 and -23‰ PDB. No distinct difference is observed in the stable isotope composition of fault or vein cement, concretions, and pore-filling calcite cement forming cement halos around joints. Figure 11b, plotting our own carbon isotope analyses as a function of distance from major fault segments of the Moab fault system, shows that the lightest $\delta^{13}\text{C}$ values are within and close to the major fault segments, and the heavier values are away from the fault segments. No such systematic change was observed for corresponding oxygen isotopic

values suggesting that the observed trend in calcite $\delta^{13}\text{C}$ reflects systematic changes of the carbon pool in solution instead of a trend in precipitation temperature.

Fracture-filling calcite locally contains abundant aqueous fluid inclusions. Typically, cement growth layers rich in fluid inclusions alternate with fluid-inclusion-poor cement layers, indicating that these inclusions are primary relative to the calcite fracture cement. Care was taken to describe and analyze inclusions that were petrographically determined to have been trapped at the same time during the growth of these layers (e.g., fluid inclusion assemblages; Goldstein and Reynolds, 1994). We determined homogenization temperatures of primary inclusions in calcite sampled along fault segment 5 about 60 m (197 ft) west of its intersection with segment 1 (Figures 2; 4d, e). Assemblages of two-phase aqueous inclusions containing about 5 vol.% vapor in earlier calcite of intermediate to high inclusion density homogenize at 100–125°C. These temperatures displayed no systematic variation from the inner to outer zones of the calcite. Laser Raman microprobe analyses indicate that the vapor phase contains no CO₂ or CH₄. Assuming a hydrostatic pore-fluid pressure gradient, a minimum pressure correction for a maximum burial depth of 2 km (1.2 mi) (Garden et al., 2001) would be no more than +10°C for these inclusions. Thus, the measured homogenization temperatures are used to approximate the formation temperatures. Temperatures of final ice melting of -0.3 to -0.5°C indicate water salinities of less than 1 wt.% NaCl equivalent (Bodnar, 1993). Later, inclusion-poor calcite contained two very large (~40 μm) primary two-phase inclusions with homogenization temperatures of about 84°C among more abundant small (<7 μm) single-phase aqueous primary inclusions, suggesting that smaller inclusions were in a metastable state. Some calcite-containing primary two-phase inclusions are twinned, indicating that the deformation outlasted the precipitation of higher temperature calcite. The $\delta^{18}\text{O}$ composition of this calcite was measured at -22.77‰ PDB. Over the range of measured homogenization temperatures (84–125°C), this corresponds

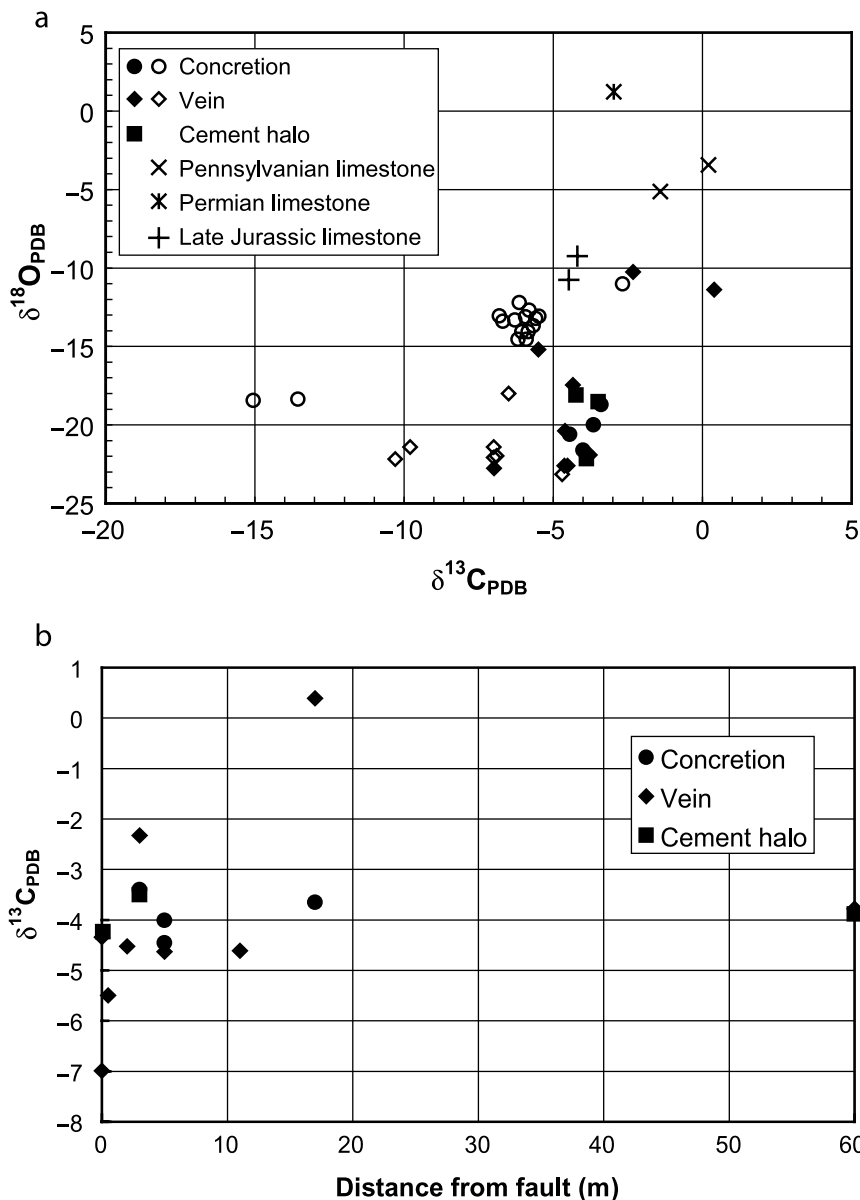


Figure 11. (a) Oxygen and carbon isotopic composition of fault and vein calcite cement, calcite concretions, and pore-filling calcite cement within cement halos along fractures. Additional analyses by Chan et al. (2000) for vein cement in the Courthouse Rock area (open diamonds) and by Garden et al. (2001) for concretions (open circles) and three limestones in the Moab-Arches National Park area. (b) Carbon isotopic composition of fault and vein calcite cement, concretions, and cement halos as a function of distance to segments of the Moab fault system. PDB = PeeDee belemnite.

to fluid $\delta^{18}\text{O}$ values from -11.4 to -7.2% standard mean ocean water (SMOW) (Friedman and O'Neil, 1977). The oxygen isotopic composition and the fluid-inclusion salinity of this sample therefore indicate a dominantly meteoric fluid composition.

At the Mill Canyon extensional step, small (1–5 μm) single-phase aqueous inclusions are common along the dust rim of quartz overgrowth cement and less common within the overgrowth. Single-phase aqueous inclusions are indicative of cement precipitation at less than 60°C (Goldstein and Reynolds, 1994).

FAULT-ROCK PETROPHYSICS

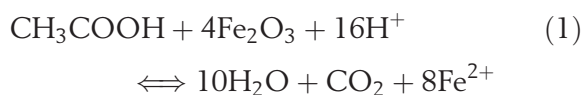
Helium porosity and air permeability were measured for twenty 1-in. (2.5-cm) core plugs sampled at Courthouse Rock and at the Mill Canyon step (Figures 5d, 8a). Core plugs taken from the fault core contain multiple parallel deformation bands but no joints or slip surfaces and were drilled and tested perpendicular to the bands. Outside the fault core, core plugs were sampled away from joints and outside calcite concretions, cement halos, or deformation bands. These samples were drilled and tested perpendicular to bedding. Analyses were

performed at Corelab Bakersfield, California, at 400-psi (2.76 MPa) confining pressure. At both sample locations, lowest porosity values of 2–7% and permeability values of less than 0.01 md were obtained from samples adjacent to the main trace of the fault. Permeability and porosity values increase to background values of 17–20% and 200–700 md, respectively, over a distance of up to 10 m (33 ft) away from the main fault strand at Courthouse Rock and outside the step region at Mill Canyon. The largest values of 23% and 911 md, however, were measured within the fault damage zones, adjacent to samples with the lowest values. The heterogeneity in helium porosity within the fault damage zone is consistent with observed variations in porosity in thin sections from the fault damage zone (e.g., Figure 3h).

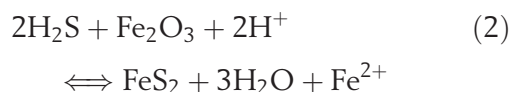
DISCUSSION

The Association of Hydrocarbons, Bleaching, and Calcite Precipitation

Based on the common occurrence of residual hydrocarbons along the Moab fault and associated subsidiary faults, extensive bleaching of the red Jurassic sandstones was attributed to the chemical interaction of hydrocarbons with hematite-cemented sandstone by Garden et al. (1997), Chan et al. (2000), and Garden et al. (2001). Because of the low solubility of hematite in oil, bleaching of hematite-cemented sandstone is more likely to result from the interaction of rock with reducing aqueous fluid that may have been in contact with hydrocarbons or organic-rich reducing shale units instead of direct oil-rock interaction. Two possible bleaching reactions are



for the reaction of hematite with organic acids, and



for the reaction of hematite with hydrogen sulfide (Garden et al., 1997; Chan et al., 2000).

Organic acids such as acetic acid are frequently abundant in oil-field waters (Franks et al., 2001) and are effective in dissolving silicates such as plagioclase (Crossey et al., 1986). Evidence of feldspar dissolution was observed within the Mill Canyon extensional step (Figure 4c). Organic acids form during catagenesis of organic matter (Lewan and Pittman, 1994) but may also be derived from the oil phase at water-oil contacts by aerobic and anaerobic microbial oxidation (Cozzarelli et al., 1990; Boles, 1992; Helgeson et al., 1993; Watson et al., 2002).

Both hematite reduction reactions consume protons and would thus increase the pH. These reactions would thus favor calcite precipitation, which is consistent with the observed preferred occurrence of calcite in bleached zones. The close association of calcite and bleaching is illustrated in Figure 4f showing calcite precipitation along joints in the sandstone, whereas the same joints are associated with bleaching halos in the underlying red siltstone. This association of bleaching and calcite precipitation may also be explained by the combined effects of organic acid production and dissociation. Organic acids dissociate readily to CO_2 and CH_4 (Bell and Palmer, 1994). In the presence of organics acids, the production of CO_2 may increase alkalinity and lead to calcite precipitation (Surdam and Crossey, 1985). The formation of acids caused by the breakdown of hydrocarbons would tend to mobilize calcite by reducing pH, whereas bleaching of hematite and the dissociation of organic acids would promote calcite precipitation. The effect of the organic acid buffer is dependent on acid concentration. Variations in fluid composition may lead to alternating stages of carbonate dissolution and precipitation (Eichhubl and Boles, 2000a).

A possible scenario that accounts for bleaching of hematite-stained red sandstone, calcite precipitation, and hydrocarbons consists of oil migrating up along faults; organic acids either migrate in solution up along the fault with a separate formation water phase or form in situ at water-oil contacts, bleaching red sandstone adjacent to the fault

system by dissolving hematite; hematite dissolution and the subsequent dissociation of organic acids would favor calcite precipitation. This mechanism allows for the formation and dissociation of organic acids to be spatially and temporally associated with bleaching of red sandstone and the precipitation of calcite.

Carbonate cementation in response to microbial oxidation of hydrocarbons is well documented and includes pore-filling carbonate along contacts of petroleum reservoirs (Macaulay et al., 2000), fault cements (Eichhubl and Boles, 2000a; Boles et al., 2004), cements associated with natural hydrocarbon microseeps (Donovan, 1974; Donovan et al., 1974; Gunatilaka, 1989), and cements associated with hydrocarbon spills (Tuccillo et al., 1999). These cements are generally understood to be frequently highly depleted in ^{13}C , reflecting the isotopically light carbon pool in the oil and gas phase. For instance, massive fault calcite cement with $\delta^{13}\text{C}$ of -30 to -40‰ PDB was ascribed by Boles et al. (2004) to the oxidation of methane migrating up along the Refugio fault from a nearby natural gas reservoir in southern California. Similarly, light carbon isotopes for carbonate cements in North Sea reservoirs were reported by Macaulay et al. (2000) and attributed to methane oxidation.

The $\delta^{13}\text{C}$ composition of calcite cement along the Moab fault of 0 to -15‰ PDB reported in this study and by Chan et al. (2000) and Garden et al. (2001) is clearly distinct from these isotopically light methanogenic carbonates. Based on the carbon isotopic composition and the shape of carbonate deposits in the crest of the Moab anticline adjacent to the Moab fault, Haszeldine et al. (2005) dismissed a hydrocarbon source for these carbonates. Instead, these authors suggested carbonate deposition in association with upward-migrating mantle-derived CO_2 , accompanied by bleaching of red sandstone by CO_2 - and H_2S -rich waters. Although subsurface CO_2 reservoirs in the Colorado Plateau region are dominated by magmatic, and possibly mantle, CO_2 (Gilfillan et al., 2008), spring waters have a variable, although generally elevated, magmatic CO_2 component (Crossey et al., 2006). Based on carbon isotopic analyses of these waters, Crossey et al. (in press) inferred

that the carbon pool is dominated by inorganic carbon derived from carbonate dissolution, with a lesser magmatic component, and a minor soil CO_2 component. Calcite vein and travertine deposits associated with natural CO_2 seepage along the nearby Little Grand Wash and Salt Wash faults have a carbon isotopic composition of $+4$ to $+9\text{‰}$ PDB (Shipton et al., 2004), distinctly heavier than the values reported for the Moab fault in the Courthouse Rock area.

Despite the, at first sight, ambiguous carbon isotope values, the consistent spatial association of calcite with residual oil or bitumen in the Courthouse Rock area is indicative of an association of hydrocarbons with calcite precipitation. Concretionary cement growth around oil nuclei (Figure 3d, e) indicates a strong seed effect for cement nucleation, which can be explained by the localized microbial activity on the oil-water contact of residual oil globules in the porous sandstone, conditions similar to those found in microseeps and oil spills. Donovan (1974) and Donovan et al. (1974) described systematic carbon isotopic trends around microseeps, with $\delta^{13}\text{C}$ values of carbonate increasing from -40‰ PDB close to the migration conduits to as high as -5‰ PDB at the periphery. A similar zonation in isotopic composition of inorganic carbon dissolved in groundwater surrounding an oil spill was described by Baedeker et al. (1993), with $\delta^{13}\text{C}$ values ranging from -22‰ to as high as -4‰ PDB within the anoxic zone surrounding the spill. These isotopic trends reflect a complex sequence in microbial degradation of oil, including methanogenesis in the anoxic zone, reduction of Fe^{3+} , organic acid production and subsequent microbial consumption, and precipitation of Fe-rich carbonate, with microbial associations and redox conditions variable on the submeter scale (Cozzarelli et al., 1990; Bennett et al., 1993; Tuccillo et al., 1999; Bekins et al., 2001; Watson et al., 2002). These steps may include fermentation of organic acids producing carbonate highly enriched in ^{13}C under anaerobic conditions (Dimitrakopoulos and Muehlenbachs, 1987). Boles (1998) attributed isotopically heavy late carbonate pore cements in the San Joaquin Basin of California ($\delta^{13}\text{C}$ up to $+16\text{‰}$) to fermentation of

organic acids containing carboxyl carbon as heavy as +8‰ (Franks et al., 2001).

Similar to the isotopic zonation observed around microseeps and spills, the carbon isotopic composition of calcite in the Courthouse Rock area is lowest for cement contained within major fault segments (Figure 10b), consistent with more reducing conditions along faults because of higher abundance of oil and higher microbial activity. We suggest that, with increasing distance from faults, the carbon pool was increasingly dominated by isotopically heavier carbon in solution within the groundwater aquifer, derived primarily from carbonate dissolution with a lesser igneous and soil carbon component, with the possible addition of heavy carbon from acid fermentation. This increasing groundwater carbon component resulted in an increasingly heavier carbon isotopic composition in cement farther from the fault. In the fault damage zone, the occurrence of calcite cement along joints and within concretions may have been controlled by more reducing microenvironments around globules and pockets of hydrocarbon providing conditions more conducive for calcite precipitation, similar to processes envisioned by Gunatilaka (1989) for the formation of microseep-related dolomite concretions in Kuwait. The heterogeneity in carbon isotopic compositions implied by this model is reflected in Figure 11b where the lowest carbon isotopic ratios occur adjacent to the fault, becoming increasingly heterogeneous at greater distance. The carbon isotopic composition of the damage-zone calcites reflects the mixed carbon pool in the surrounding pore water that contains a large groundwater signature that progressively dominates at increasing distance from the fault.

Fluid-Flow Conditions Associated with Fault-Related Cementation

Based on the inferred chemical environment of microbial hydrocarbon oxidation and calcite precipitation, we envision that the fluid environment is volumetrically dominated by meteoric water contained in the Jurassic aquifer, with a minor basinal fluid component migrating up along the fault system within conduits of higher permeability or

fault pipes (Eichhubl and Boles, 2000a). The dominant meteoric fluid component over deep basinal fluids in the damage zone is consistent with the low salinity of fluid inclusions and the light oxygen isotopic composition, suggesting a water $\delta^{18}\text{O}$ composition ranging from -11.4 to -7.2‰ SMOW. Modern meteoric water in this area has a $\delta^{18}\text{O}$ composition of -15 to -12‰ SMOW (Spangler et al., 1996). The smaller basinal fluid component likely provided the source of Cu and Ba for the precipitation of malachite and barite cements, respectively.

The hydraulic significance of the fault-flow conduits can be illustrated by estimating the volume of the aqueous solution involved in the precipitation of calcite at the Courthouse Rock intersection. The following mass balance is based on the volume of calcite determined earlier and on the assumption that the mass of precipitated calcite was limited by the availability of calcium cations. Spangler et al. (1996) gave an average Ca^{2+} concentration of 20 mg/L for meteoric water in the Navajo aquifer and of 5000 mg/L for saline oil field brines. Precipitation of 800 m³ (28,252 ft³) of calcite at the Courthouse intersection requires therefore a minimum of 0.2×10^9 L of brine or 40×10^9 L of meteoric water, or a water/rock ratio of about 200:1 to 50,000:1. Considering that the oxygen isotopic composition of calcite indicates a dominant meteoric water component, the required volume of water for calcite precipitation at the Courthouse intersection is likely to be closer to the upper estimate. These values are minimum estimates because they assume that all Ca^{2+} contained in the aqueous solution will precipitate as calcite, which is unlikely for both thermodynamic and kinetic reasons. Eichhubl and Boles (2000a) argued that thermodynamic mass balancing may underestimate the actual fluid volume by a factor of 10.

Our estimates support the hydrogeologic model of Chan et al. (2000), which includes migration of hydrocarbons and basinal brines from Pennsylvanian source rocks up along the Moab fault and movement of hydrocarbons into the porous sandstone units where they interact with large volumes of oxygenated meteoric water. The porous

sandstone units such as the Moab Tongue and Navajo sandstones may have acted as regional aquifers allowing continuous supply of meteoric water into the vicinity of the fault. In contrast to the results by Chan et al. (2000), our fluid inclusion analyses indicate that high-temperature (84–125°C), low-salinity aqueous fluids were involved in fault calcite precipitation, consistent with deep, topographically driven circulation of meteoric water. The lower range of these temperatures is consistent with modeled maximum burial temperatures of about 90°C obtained by Garden et al. (2001). Because biodegradation of hydrocarbons is considered limited to temperatures below approximately 80°C (Larter et al., 2006), we suggest that the higher range of observed temperatures reflect focused flow of hot fluid, with microbial activity occurring along the cooler periphery of the flow conduits. The fluid-inclusion temperatures would thus represent temperatures that are elevated relative to the ambient formation temperature. Clastic dikes in the footwall of the fault system suggest episodic and possibly seismic upward flow of deeper sourced and confined fluid along the fault into an unconfined meteoric aquifer.

The proposed mechanism of fault-related calcite precipitation associated with the volumetrically limited migration of hydrocarbons and their biodegradation differs from carbonate fault cementation by CO₂ exsolution during the rapid upward flow of basinal brine or CO₂-saturated groundwater. This mechanism can result in massive carbonate deposits as observed at the nearby Little Grand Wash and Salt Wash faults (Shipton et al., 2004) and in the Monterey Formation of California (Eichhubl and Boles, 2000b). This mechanism also differs in isotopic composition, occurrence, and mass of cement from the massive calcite deposits described by Boles et al. (2004) along the Refugio fault in California, which they attributed to oxidation of large volumes of migrating methane.

A deeply circulating meteoric recharge system in the vicinity of the Moab fault system is in agreement with findings by Pevear et al. (1995) of ¹⁸O-depleted illite in the fault zone, yielding 50-Ma K-Ar ages. In this model, basinal brine and hydro-

carbons form a volumetrically minor component of fluid flow along the fault. Chan et al. (2001) suggested a possible link between the onset of such deep meteoric circulation with the Oligocene uplift of the La Sal Mountains to the southeast.

Basin models by Garden et al. (2001) indicate that the maximum burial was reached around 70 Ma, and maximum burial temperatures of about 90°C for the Middle and Upper Jurassic sections were reached at around 40 Ma. Earlier basin models by Nuccio and Condon (1996) suggested maximum burial and maximum temperature conditions of 90°C at 38 Ma. Vrolijk and van der Pluijm (1999) inferred temperatures of 100°C (±10°) based on vitrinite, illite/smectite, and fission-track paleothermometry. These temperature estimates would confirm that higher temperature flow was focused along high-permeability conduits. Based on Ar dating of illite-smectite in the fault gouge, Solum et al. (2005) determined a Paleocene age of most recent fault motion.

These age constraints compare well with paleomagnetic results by Garden et al. (2001), suggesting reduction of iron oxides and remagnetization during the Paleogene (63–49 Ma). The meteoric flow regime in the exposed Jurassic sandstone units in the Courthouse area was likely active until the incision of the Colorado River drainage and erosion in the Pleistocene (Hurlow and Bishop, 2003).

Because quartz overgrowth cement at the extensional Mill Canyon step predates calcite cement, single-phase inclusions in quartz overgrowth cement are interpreted to record earlier fault-associated fluid flow at temperatures less than 60°C. Following Garden et al. (2001), the 60°C isotherm was crossed by the Upper Jurassic units around 90 Ma.

Structural Control of Fluid Flow and Implications for Fault Sealing

The Moab fault illustrates the complex fault-fluid-flow properties and their spatial variation as a function of fault-zone architecture. Because of the juxtaposition of sandstone against shale layers and the entrainment of shale along the fault

(Davatzes and Aydin, 2005), cross-fault flow will be impeded in the central part of the Moab fault. This is consistent with groundwater well data presented by Hurlow and Bishop (2003) who concluded that the fault zone in the Courthouse–Sevenmile Canyon area is a barrier for modern groundwater flow in near-surface aquifers. Although fault juxtaposition models by Clarke et al. (2005) identified segment 1 in the Courthouse Rock area as a potential leak point for cross-fault fluid flow based on shale/gouge ratio calculations, we did not find diagenetic field evidence to support cross-fault fluid flow in this area. The hanging wall of fault segment 1 in this area consists of a greater than 6-m-thick (20-ft-thick) layer of entrained Jurassic shale, separating Cretaceous sandstone in the hanging wall from Jurassic sandstone in the footwall along segment 1 (Davatzes and Aydin, 2005) (Figures 5a, 6). Eichhubl et al. (2005) demonstrated that shale entrainment can result in a higher sealing capacity of faults compared to shale/gouge ratio calculations.

The diagenetic record also suggests the absence of fault-parallel fluid flow along segments composed solely of deformation bands. This includes most of segment 1 in the study area and parts of segment 2 that are located away from fault intersections and steps (Figure 2). Although slip surfaces along these segments may be considered potential flow pathways for fault-parallel flow, such flow, if any, is not expressed in the diagenetic record.

The preferred occurrence of calcite cement in areas of increased joint density (Figures 3–5) indicates that joints acted as preferred flow conduits in the fault damage zone and in the fault core where they are composed of joints and fault breccia. The observed trend in carbon isotopes adjacent to fault segment 2a, with lowest $\delta^{13}\text{C}$ values measured in veins within the brecciated fault core (Figure 11b), suggests that the upward flow of basinal fluid and deeply circulating meteoric water was focused in the brecciated fault core. Connected joints in the damage zone within a few meters adjacent to the fault allowed flow away from the fault conduit and mixing of upward-flowing fluids with ambient meteoric water, providing conditions for hydrocarbon degradation and calcite precipitation.

Based on elastic boundary element models of stress magnitudes and directions in the vicinity of fault intersections, Davatzes et al. (2003) demonstrated that joint density is correlated with changes in magnitude of the least principal stress that are induced by fault interactions at segment intersections and steps. Loading conditions for these numerical models were chosen to match slip directions on the fault segments in agreement with fault striation observations, without any additional a priori constraints on stress orientations and stress magnitudes. However, the best-fitting models were consistent with the inferred burial depth of 2 km (1.2 mi) following Garden et al. (2001). In the case of the Courthouse intersection, a large drop in the least compressive principal stress is found north of segment 2b where a high joint density and calcite occurrence were observed in the field (Figure 12). Joint orientation coincides with the computed orientations of the minimum compressive principal stress. Similar correlations between observed joint density and orientation and computed stress field apply to the extensional fault step east of Mill Canyon, the fault intersections west of Mill Canyon, and the termination of fault segment 4 west of Mill Canyon (Figure 13) (see Davatzes et al., 2003, for numerical solutions). Numerical simulations of the contractional step west of Mill Canyon show more compressive minimum principal compressive stresses and more compressive mean stresses consistent with the lack of joints and a high density of deformation bands. The contractional fault step west of Mill Canyon lacks preferred calcite cementation.

Following Davatzes et al. (2003), joints, where present along the fault zone, overprint and postdate earlier fault structures composed of deformation bands. The joint-based deformation mechanism and the resultant increase in fault permeability therefore characterize a more developed stage of faulting on a given fault segment. This switch in deformation mechanism, which may have occurred at different times for different fault segments, probably relates to changes in stress state within the fault zone and changes in diagenetic state of the host sequence, as discussed by Davatzes et al. (2003) for the Chimney fault array in central Utah. The stress

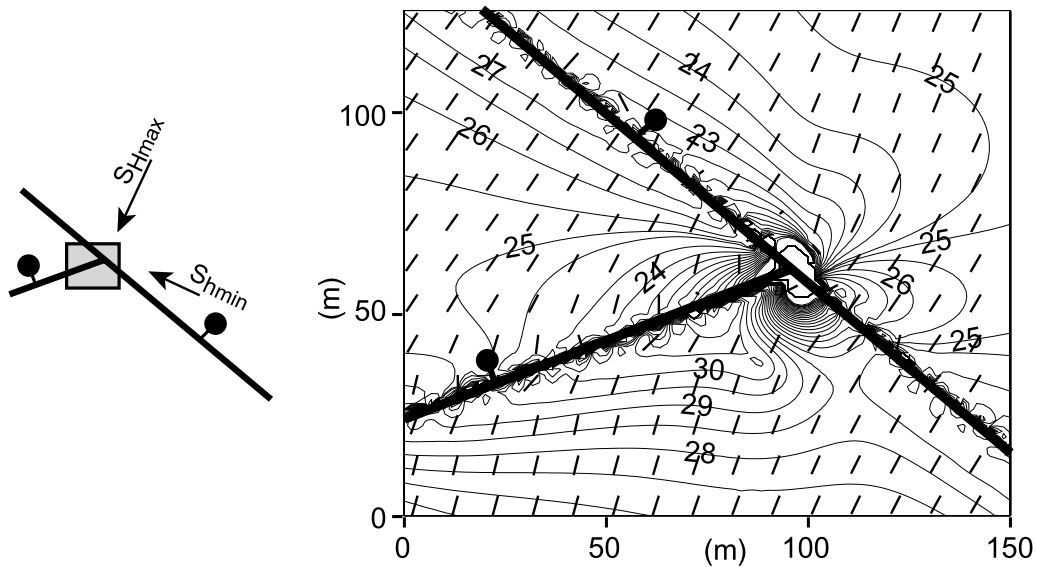


Figure 12. Elastic boundary element model illustrating the magnitude of the least principal stress around a fault intersection. Fault geometry is selected to approximate the geometry observed at Courthouse Rock (Figure 5). Orientation and magnitudes of the loading stress state were chosen to match the relative slip magnitude and slip direction as observed in the field. Tick marks indicate the trace of maximum horizontal stress (S_{Hmax}). The contour interval is 0.5 MPa; compression is positive. Areas of low magnitudes in the least principal stress coincide with areas of enhanced opening-mode fracture density in sandstone and increased abundance of calcite cement as mapped in Figure 5b and a, respectively. S_{Hmin} = minimum horizontal stress.

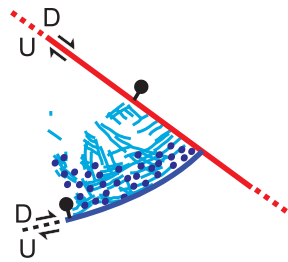
state within the fault zone will be controlled by tectonic loading conditions, ambient confining stress, and local stress perturbations caused by fault segment interaction. The stress state within the fault zone is thus in part controlled by fault-segment geometry as illustrated by our numerical simulations, with the geometry controlled by the initial nucleation and the growth of fault segments and their coalescence with increasing fault slip. In addition, if faulting continued into the stage of fault exhumation, the accompanying decrease in mean stress would further promote joint formation. Stress dependence in deformation mechanism is consistent with the systematic occurrence of joints along extensional parts of fault segments. This switch does not appear to be a linear function of fault throw because joints and calcite cement are equally well developed along fault segments with lesser throw (e.g., segments 4, 5, and 6). The increase in fault-parallel permeability with increasing fault-zone development is consistent with independent estimates of Tertiary-age fault-related chemical alteration summarized in the preceding section.

The increased abundance of quartz overgrowth cement at the extensional Mill Canyon step pre-

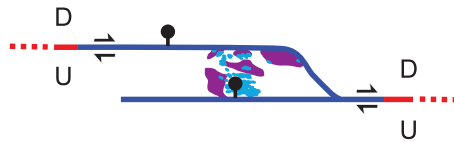
dates jointing because joints crosscut quartz overgrowth cement. We attribute the increase in quartz cement adjacent to segment 2b to the advective transport of heat and possibly silica. Increased abundance of quartz overgrowth cement caused by higher fluid temperature within and adjacent to the fault would be consistent with current models of quartz cement precipitation in sedimentary basins (Lander and Walderhaug, 1999). A similar occurrence of fault-related quartz overgrowth cement was described by Quinn and Haszeldine (2004) from the Inner Moray Firth Basin, United Kingdom, and attributed to ascending fluids. Because fluid inclusions in quartz overgrowth cement at the Mill Canyon extensional step are single phase, we could not test for systematic variations in fluid temperature with distance from the fault. Cataclasis associated with deformation band formation may potentially enhance quartz dissolution and reprecipitation, but quartz cement is not noticeably more abundant at the contractional Mill Canyon step, which is characterized by high deformation band density.

Unlike quartz cement at the extensional fault step, which precedes jointing, calcite cement at

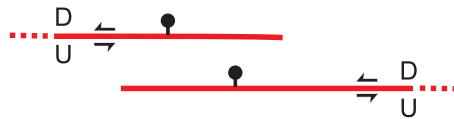
Fault segment intersection



Fault step extensional



contractional



Fault termination



- Deformation band fault
- Joint-based fault (overprinting deformation bands)

- Carbonate veins and concretions
- Quartz cementation

Figure 13. Occurrence of fault-related diagenesis relative to fault-segment boundaries along the Moab fault (map view).

the fault intersections appears to postdate joint formation. Joints thus likely enhanced the flow of hydrocarbons from the fault into the surrounding formation where microbial hydrocarbon degradation in contact with meteoric water resulted in enhanced calcite precipitation. The preferred occurrence of calcite cement in the Moab Tongue sandstone may reflect the high permeability of this unit allowing the interaction of hydrocarbons with large volumes of meteoric water. In addition, the overlying shale of the Tidwell Member of the Morrison Formation likely acted as a top seal that resulted in the pooling of buoyant hydrocarbons where they chemically interacted with meteoric water flowing along the porous and permeable Moab Tongue sandstone.

Based on the clay compositional zonation of the fault zone in the central part of the Moab fault, with more permeable illite-rich clays in the fault core and less permeable smectite-rich clays in the fault damage zone, Solum et al. (2005) suggested that the fault core is hydraulically more conductive for fault-parallel flow than the fault damage zone. Our field structural and diagenetic observations in the Courthouse segment suggest that the fractured fault damage zone in sandstone is most conductive for fault-parallel fluid flow.

The preferred fault-parallel flow in the fault core as inferred by Solum et al. (2005) may characterize structural levels lower than those exposed in the Courthouse area, where finer grained units of the Triassic Moenkopi and Chinle formations abut the fault.

Calcite precipitation resulting from microbial interaction of migrating hydrocarbons with meteoric water could be seen as a mechanism of self-sealing along leaking hydrocarbon fault conduits. Although fault breccias appear effectively sealed by calcite cement (Figure 4d), joints in the fault damage zone are only incompletely sealed. Veins and associated cement halos are typically discontinuous (Figure 3d), leaving sections of joints uncemented. We attribute the discontinuous occurrence of calcite cement to the discontinuous distribution of oil within fractures, providing a blueprint for the discontinuous distribution of calcite-precipitating microbes. Liesegang patterns centered around uncemented joint segments (Figure 4b) are indicative of preferred fluid flow along these joint segments. The incomplete cementation by calcite is likely to be characteristic of microbially mediated cementation processes, reflecting the discontinuous distribution of hydrocarbons within the joint systems adjacent to the major fault segments.

These discontinuous cements may thus impede fluid flow, forcing flow from the fault conduits into the damage zone, while remaining inefficient in forming a continuous fault seal. The effect of the discontinuous fault-related cementation is enhanced by the heterogeneous distribution of core-plug porosity and permeability. Because calcite-cemented zones were avoided for core-plug measurements, the heterogeneity captured by these measurements will act in addition to the cement heterogeneity. In fact, the distribution of calcite and quartz cement may, in part, have been controlled by the heterogeneity in mechanical porosity reduction in the fault damage zone.

The rather ineffective processes of diagenetic sealing observed along the Moab fault and ascribed here to volumetrically limited migration of hydrocarbons and their microbial degradation differ from extensive and massive carbonate cementation observed at other fault systems and attributed to rapid upward fluid flow, decompression, and CO₂ exsolution. Carbonate precipitation by rapid CO₂ exsolution will be less dependent on seed effects because of the high supersaturation of the aqueous solution, thus allowing for continuous and extensive precipitation of carbonate in the fault core and fault damage zone. Yet, despite their differences in sealing capacity, both processes of fault-related cementation are controlled by the availability of open and connected fracture systems. For both types of fault cementation, cement will preferentially precipitate at dilatational fault segments, intersections, and terminations.

CONCLUSIONS

Diagenetic alteration in Jurassic porous sandstone along the Moab fault provides a proxy for the structural control of focused flow along the segmented fault system. Fault-controlled diagenesis includes calcite precipitation in the form of concretions, veins, and cement halos; iron oxide dissolution and reprecipitation; and locally increased abundance of quartz overgrowth cementation. Diagenetic alteration is localized in areas of structural complexity that include extensional steps,

fault intersections, and fault terminations. These areas are structurally characterized by a high density of joints that overprint earlier deformation bands. We find that high joint density and thus high fault-parallel permeability correlate with areas of less compressive stress states within the fault zone, with the stress state strongly affected by mechanical fault-segment interaction. With increasing fault development and thus increasing mechanical fault-segment interaction, fault permeability increases, albeit at different rates and extent for different segments of the fault system.

Based on the association of calcite cement with residual oil, in conjunction with the stable isotopic and fluid-inclusion composition of calcite cement, we infer that calcite precipitation resulted from the microbial oxidation of hydrocarbons that migrated up along the fault into a meteoric aquifer. Calcite fracture cement is typically discontinuous, presumably reflecting the discontinuous distribution of oil in the fault damage zone and resulting in the inefficient diagenetic sealing of the fault-flow conduits. Although cross-fault flow is controlled by shale juxtaposition and entrainment along the fault, fault-parallel flow is controlled by the complex interplay of fault loading conditions, host lithology, and resultant fault architecture, and by the effects of fluid chemical environment on the type and distribution of diagenetic alteration products.

REFERENCES CITED

- Allan, U. S., 1989, Model for hydrocarbon migration and entrapment within faulted structures: *AAPG Bulletin*, v. 73, p. 803–811.
- Antonellini, M. A., and A. Aydin, 1994, Effect of faulting on fluid-flow in porous sandstones—Petrophysical properties: *AAPG Bulletin*, v. 78, p. 355–377.
- Aydin, A., 2000, Fractures, faults, and hydrocarbon migration and flow: *Marine and Petroleum Geology*, v. 17, p. 797–814, doi:10.1016/S0264-8172(00)00020-9.
- Baedecker, M. J., I. M. Cozzarelli, R. P. Eganhouse, D. I. Siegel, and P. C. Bennett, 1993, Crude oil in a shallow sand and gravel aquifer: III. Biogeochemical reactions and mass balance modeling in anoxic groundwater: *Applied Geochemistry*, v. 8, p. 569–586, doi:10.1016/0883-2927(93)90014-8.
- Bekins, B. A., I. M. Cozzarelli, E. M. Godsy, E. Warren, H. I. Essaid, and M. E. Tuccillo, 2001, Progression of natural

- attenuation processes at a crude-oil spill site: II. Controls on spatial distributions of microbial populations: *Journal of Contaminant Hydrology*, v. 53, p. 387–406, doi:10.1016/S0169-7722(01)00175-9.
- Bell, J. L. S., and D. A. Palmer, 1994, Experimental studies of organic acid decomposition, in E. D. Pittman and M. D. Lewan, eds., *Organic acids in geological processes*: Berlin, Springer, p. 226–269.
- Bennett, P. C., D. I. Siegel, M. J. Baedeker, and M. F. Hult, 1993, Crude oil in a shallow sand and gravel aquifer: I. Hydrogeology and inorganic geochemistry: *Applied Geochemistry*, v. 8, p. 529–549, doi:10.1016/0883-2927(93)90012-6.
- Berg, S. S., and T. Skar, 2005, Controls on damage zone asymmetry of a normal fault zone: Outcrop analyses of a segment of the Moab fault, southeastern Utah: *Journal of Structural Geology*, v. 27, p. 1803–1822, doi:10.1016/j.jsg.2005.04.012.
- Bodnar, R. J., 1993, Revised equation and table for determining the freezing point depression of H₂O–NaCl solutions: *Geochimica et Cosmochimica Acta*, v. 57, no. 3, p. 683–684, doi:10.1016/0016-7037(93)90378-A.
- Boles, J. R., 1992, Evidence for oil-derived organic acids in reservoirs, in Y. K. Kharaka and A. S. Maest, eds., *Water-rock interaction: Proceedings of 7th International Symposium*, Park City, Utah, p. 311–314.
- Boles, J. R., 1998, Carbonate cementation in Tertiary sandstones, San Joaquin Basin, California, in S. Morad, ed., *Carbonate cementation in sandstones: Distribution patterns and geochemical evolution*: International Association of Sedimentologists Special Publication 26, p. 261–283.
- Boles, J. R., P. Eichhubl, G. Garven, and J. Chen, 2004, Evolution of a hydrocarbon migration pathway along basin-bounding faults: Evidence from fault cement: *AAPG Bulletin*, v. 88, no. 7, p. 947–970, doi:10.1306/02090403040.
- Breit, G. N., M. B. Goldhaber, D. R. Shawe, and E. C. Simmons, 1990, Authigenic barite as an indicator of fluid movement through sandstones within the Colorado Plateau: *Journal of Sedimentary Petrology*, v. 60, p. 884–896.
- Chan, M. A., W. T. Parry, and J. R. Bowman, 2000, Diagenetic hematite and manganese oxides and fault-related fluid flow in Jurassic sandstones, southern Utah: *AAPG Bulletin*, v. 84, p. 1281–1310.
- Chan, M. A., W. T. Parry, E. U. Petersen, and C. M. Hall, 2001, ⁴⁰Ar/³⁹Ar age and chemistry of manganese mineralization in the Moab and Lisbon fault systems, southeastern Utah: *Geology*, v. 29, p. 331–334, doi:10.1130/0091-7613(2001)029<0331:AAAACO>2.0.CO;2.
- Clarke, S. M., S. D. Burley, and G. D. Williams, 2005, A three-dimensional approach to fault seal analysis: Fault-block juxtaposition and argillaceous smear modeling: *Basin Research*, v. 17, p. 269–288, doi:10.1111/j.1365-2117.2005.00263.x.
- Cozzarelli, I. M., R. P. Eganhouse, and M. J. Baedeker, 1990, Transformation of monoaromatic hydrocarbons to organic acids in anoxic groundwater environment: *Environmental Geology and Water Sciences*, v. 16, p. 135–141, doi:10.1007/BF01890379.
- Crossey, L. J., R. C. Surdam, and R. Lahann, 1986, Application of organic/inorganic diagenesis to porosity prediction, in D. L. Gautier, ed., *Roles of organic matter in sediment diagenesis*: SEPM Special Publication 38, p. 147–155.
- Crossey, L. J., T. P. Fischer, P. J. Patchett, K. E. Karlstrom, D. R. Hilton, D. L. Newell, P. Huntoon, A. C. Reynolds, and G. A. M. de Leeuw, 2006, Dissected hydrologic system at the Grand Canyon: Interaction between deeply derived fluids and plateau aquifer waters in modern springs and travertine: *Geology*, v. 34, p. 25–28, doi:10.1130/G22057.1.
- Crossey, L. J., K. E. Karlstrom, A. Springer, D. Newell, D. R. Hilton, and T. Fischer, in press, Degassing of mantle-derived CO₂ and ³He from springs in the southern Colorado Plateau region—Flux rates, neotectonic connections, and implications for groundwater systems: *Geological Society of America Bulletin*.
- Davatzes, N. C., and A. Aydin, 2003, Overprinting faulting mechanisms in sandstone: *Journal of Structural Geology*, v. 25, p. 1795–1813, doi:10.1016/S0191-8141(03)00043-9.
- Davatzes, N. C., and A. Aydin, 2005, Distribution and nature of fault architecture in a layered sandstone and shale sequence: An example from the Moab fault, Utah, in R. Sorkhabi and Y. Tsuji, eds., *Faults, fluid flow, and petroleum traps*: AAPG Memoir 85, p. 153–180.
- Davatzes, N. C., A. Aydin, and P. Eichhubl, 2003, Overprinting faulting mechanisms during the development of multiple fault sets in sandstone, Chimney Rock fault array, Utah, U.S.A.: *Tectonophysics*, v. 363, no. 1–2, p. 1–18, doi:10.1016/S0040-1951(02)00647-9.
- Davatzes, N. C., P. Eichhubl, and A. Aydin, 2005, Structural evolution of fault zones in sandstone by multiple deformation mechanisms: Moab fault, southeastern Utah: *Geological Society of America Bulletin*, v. 117, no. 1–2, p. 135–148, doi:10.1130/B25473.1.
- Dimitrakopolous, R., and K. Muehlenbachs, 1987, Biodegradation of petroleum as a source of ¹³C-enriched carbon dioxide in the formation of carbonate cement: *Chemical Geology (Isotope Geoscience Section)*, v. 65, p. 283–291.
- Doelling, H. D., 2003, Geology of Arches National Park, Utah, in D. A. Sprinkel, T. C. Chidsey Jr., and P. B. Anderson, eds., *Geology of Utah's parks and monuments*, 2d ed.: Utah Geological Association Publication 28, p. 11–36.
- Doelling, H. H., 1985, Geology of Arches National Park: Accompaniment to Utah Geological Survey Map 74, 15 p., scale 1:50,000, 1 sheet.
- Doelling, H. H., 1988, Geology of Salt Valley anticline and Arches National Park, Grand County, Utah, in H. H. Doelling, C. G. Oviatt, and P. W. Huntoon, eds., *Salt deformation in the Paradox region*: Utah Geological and Mineral Survey, Bulletin 122, p. 1–60.
- Donovan, T. J., 1974, Petroleum microseepage at Cement, Oklahoma—Evidence and mechanisms: *AAPG Bulletin*, v. 58, p. 429–446.

- Donovan, T. J., I. Friedman, and J. D. Gleason, 1974, Recognition of petroleum-bearing traps by unusual isotopic composition of carbonate-cemented surface rocks: *Geology*, v. 2, p. 351–354, doi:10.1130/0091-7613(1974)2<351:ROPTBU>2.0.CO;2.
- Doughty, P. T., 2003, Clay smear seals and fault sealing potential of an exhumed growth fault, Rio Grande rift, New Mexico: *AAPG Bulletin*, v. 87, p. 427–444, doi:10.1306/10010201130.
- Eichhubl, P., and J. R. Boles, 2000a, Focused fluid flow along faults in the Monterey Formation, coastal California: *Geological Society of America Bulletin*, v. 112, p. 1667–1679, doi:10.1130/0016-7606(2000)112<1667:FFFAFI>2.0.CO;2.
- Eichhubl, P., and J. R. Boles, 2000b, Rates of fluid flow in fault systems—Evidence for episodic fluid flow in the Miocene Monterey Formation, coastal California: *American Journal of Science*, v. 300, p. 571–600, doi:10.2475/ajs.300.7.571.
- Eichhubl, P., W. L. Taylor, D. D. Pollard, and A. Aydin, 2004, Paleo-fluid flow and deformation in the Aztec Sandstone at the Valley of Fire, Nevada—Evidence for the coupling of hydrogeologic, diagenetic, and tectonic processes: *Geological Society of America Bulletin*, v. 116, p. 1120–1136, doi:10.1130/B25446.1.
- Eichhubl, P., P. D'Onfro, A. Aydin, J. Waters, and D. K. McCarty, 2005, Structure, petrophysics, and diagenesis of shale entrained along a normal fault, Black Diamond Mines, California—Implications for fault seal: *AAPG Bulletin*, v. 89, p. 1113–1137, doi:10.1306/04220504099.
- Flodin, E. A., M. Gerdes, A. Aydin, and W. D. Wiggins, 2004, Petrophysical properties and sealing capacity of fault rock from sheared-joint based faults, Aztec Sandstone, Nevada, *in* R. Sorkhabi and Y. Tsuji, eds., *Faults, fluid flow, and petroleum traps*: AAPG Memoir 85, p. 197–217.
- Fossen, H., T. E. S. Johansen, J. Hesthammer, and A. Rotevatn, 2005, Fault interaction in porous sandstone and implications for reservoir management examples from southern Utah: *AAPG Bulletin*, v. 89, p. 1593–1606, doi:10.1306/07290505041.
- Fowles, J., and S. Burley, 1994, Textural and permeability characteristics of faulted, high porosity sandstones: *Marine and Petroleum Geology*, v. 11, p. 608–623, doi:10.1016/0264-8172(94)90071-X.
- Foxford, K. A., I. R. Garden, S. C. Guscott, S. D. Burley, J. J. M. Lewis, J. J. Walsh, and J. Watterson, 1996, The field geology of the Moab fault, *in* A. C. Huffman, W. R. Lund, and L. H. Godwin, eds., *Geology and resources of the Paradox Basin*: Utah Geological Association Guidebook, v. 25, p. 265–283.
- Foxford, K. A., J. J. Walsh, J. Watterson, I. R. Garden, S. C. Guscott, S. D. Burley, Q. J. Fisher, and R. J. Knipe, 1998, Structure and content of the Moab fault zone, Utah, U.S.A., and its implications for fault seal prediction, *in* G. A. K. Jones, Q. J. Fisher, and R. J. Knipe, eds., *Faulting, fault sealing and fluid flow in hydrocarbon reservoirs*: Geological Society (London) Special Publications 147, p. 87–103.
- Franks, S. G., R. F. Dias, K. H. Freeman, J. R. Boles, A. Holba, A. L. Fincannon, and E. D. Jordan, 2001, Carbon isotopic composition of organic acids in oil field waters, San Joaquin Basin, California, U.S.A.: *Geochimica et Cosmochimica Acta*, v. 65, p. 1301–1310, doi:10.1016/S0016-7037(00)00606-2.
- Friedman, I., and J. R. O'Neil, 1977, Compilation of stable isotope fractionation factors of geochemical interest: U.S. Geological Survey Professional Paper, v. 440, 12 p.
- Garden, J. R., S. C. Guscott, K. A. Foxford, S. D. Burely, J. J. Walsh, and J. Watterson, 1997, An exhumed fill and spill hydrocarbon fairway in the Entrada Sandstone of the Moab anticline, Utah, *in* J. Hendry, P. Carey, J. Parnell, A. Ruffel, and R. Worden, eds., *Migration and interaction in sedimentary basins and orogenic belts*: *Geofluids*, v. 2, p. 287–290.
- Garden, J. R., S. C. Guscott, S. D. Burely, K. A. Foxford, J. J. Walsh, and J. Marshall, 2001, An exhumed paleo-hydrocarbon migration fairway in a faulted carrier system Entrada Sandstone of southeastern Utah, U.S.A.: *Geofluids*, v. 1, p. 195–213, doi:10.1046/j.1468-8123.2001.00018.x.
- Gartrell, A., Y. Zhang, M. Lisk, and D. Dewhurst, 2004, Fault intersections as critical hydrocarbon leakage zones: Integrated field study and numerical modelling of an example from the Timor Sea, Australia: *Marine and Petroleum Geology*, v. 21, p. 1165–1179, doi:10.1016/j.marpetgeo.2004.08.001.
- Gilfillan, S. M. V., C. J. Ballentine, G. Holland, D. Blagburn, B. Sherwood Lollar, S. Stevens, M. Schoell, and M. Cassidy, 2008, The noble gas geochemistry of natural CO₂ gas reservoirs from the Colorado Plateau and Rocky Mountain provinces, U.S.A.: *Geochimica et Cosmochimica Acta*, v. 72, p. 1174–1198, doi:10.1016/j.gca.2007.10.009.
- Goldstein, R. H., and T. J. Reynolds, 1994, Systematics of fluid inclusions in diagenetic minerals: *SEPM Short Course 31*, 199 p.
- Gunatilaka, A., 1989, Spheroidal dolomites—origin by hydrocarbon seepage?: *Sedimentology*, v. 36, p. 701–710, doi:10.1111/j.1365-3091.1989.tb02094.x.
- Haszeldine, R. S., O. Quinn, G. England, M. Wilkinson, Z. K. Shipton, J. P. Evans, J. Heath, L. Crossey, C. J. Ballentine, and C. M. Graham, 2005, Natural geochemical analogs for carbon dioxide storage in deep geological porous reservoirs, a United Kingdom perspective: *Oil & Gas Science and Technology—Revue de l'Institut Français du Pétrole*, v. 60, p. 33–49.
- Helgeson, H. C., A. M. Knox, C. E. Owens, and E. L. Shock, 1993, Petroleum, oil field waters, and authigenic mineral assemblages: Are they in metastable equilibrium in hydrocarbon reservoirs?: *Geochimica et Cosmochimica Acta*, v. 57, p. 3295–3339, doi:10.1016/0016-7037(93)90541-4.
- Hurlow, H. A., and C. E. Bishop, 2003, Recharge areas and geologic controls for the Courthouse-Sevenmile spring system, western Arches National Park, Grand County, Utah: *Utah Geological Survey Special Study*, v. 108, 55 p.
- Johansen, T. E. S., H. Fossen, and R. Kluge, 2005, The impact of syn-faulting porosity reduction on damage zone

- architecture in porous sandstone: An outcrop example from the Moab fault, Utah: *Journal of Structural Geology*, v. 27, p. 1469–1485, doi:10.1016/j.jsg.2005.01.014.
- Knipe, R. J., Q. J. Fisher, G. Jones, M. R. Clennell, A. B. Farmer, A. Harrison, B. Kidd, E. McAllister, J. R. Porter, and E. A. White, 1997, Fault seal analysis: Successful methodologies, application and future direction, in P. Møller-Pedersen and A. G. Koestler, eds., *Hydrocarbon seals, importance for exploration and production*: Amsterdam, Elsevier, p. 15–38.
- Lander, R. H., and O. Walderhaug, 1999, Porosity prediction through simulation of sandstone compaction and quartz cementation: *AAPG Bulletin*, v. 83, p. 433–449.
- Larter, S., H. Huang, J. Adams, B. Bennett, O. Jokanola, T. Oldenburg, M. Jones, I. Head, C. Riediger, and M. Fowler, 2006, The controls on the composition of biodegraded oils in the deep subsurface: Part II. Geological controls on subsurface biodegradation fluxes and constraints on reservoir-fluid property prediction: *AAPG Bulletin*, v. 90, p. 921–938, doi:10.1306/01270605130.
- Lehner, F. K., and W. F. Pilaar, 1997, The emplacement of clay smears in synsedimentary normal faults: Inferences from field observations near Frechen, Germany, in P. Møller-Pedersen and A. G. Koestler, eds., *Hydrocarbon seals, importance for exploration and production*: Amsterdam, Elsevier, p. 39–50.
- Lewan, M. D., and E. D. Pittman, 1994, Introduction to the role of organic acids in geological processes, in E. D. Pittman and M. D. Lewan, eds., *Organic acids in geological processes*: Berlin, Springer, p. 1–21.
- Ligtenberg, J. H., 2005, Detection of fluid migration pathways in seismic data: Implications for fault seal analysis: *Basin Research*, v. 17, p. 141–153, doi:10.1111/j.1365-2117.2005.00258.x.
- Macaulay, C. I., A. E. Fallick, R. S. Haszeldine, and G. E. McAulay, 2000, Oil migration makes the difference: Regional distribution of carbonate cement $\delta^{13}\text{C}$ in northern North Sea Tertiary sandstones: *Clay Minerals*, v. 35, p. 73–80.
- Main, I. G., O. Kwon, B. T. Ngwenya, and S. C. Elphick, 2000, Fault sealing during deformation—Band growth in porous sandstone: *Geology*, v. 28, p. 1131–1134, doi:10.1130/0091-7613(2000)28<1131:FSDDGI>2.0.CO;2.
- Morrison, S. J., and W. T. Parry, 1986, Formation of carbonate-sulfate veins associated with copper ore deposits from saline basin brines, Lisbon Valley, Utah: Fluid inclusion and isotopic evidence: *Economic Geology*, v. 81, p. 1853–1866.
- Myers, R., and A. Aydin, 2004, The evolution of faults formed by shearing across joint zones in sandstone: *Journal of Structural Geology*, v. 26, p. 947–966, doi:10.1016/j.jsg.2003.07.008.
- Nuccio, V. F., and S. M. Condon, 1996, Burial and thermal history of the Paradox Basin, Utah and Colorado, and petroleum potential of the Middle Pennsylvanian Paradox Basin: *U.S. Geological Survey Bulletin*, 2000-O, 41 p.
- O'Brien, G. W., and E. P. Woods, 1995, Hydrocarbon-related diagenetic zones (HRDZs) in the Vulcan sub-basin, Timor Sea: Recognition and exploration implications: *Australian Petroleum Exploration Association Journal*, v. 35, p. 220–252.
- Olig, S. S., C. H. Fenton, J. McCleary, I. G. Wong, 1996, The earthquake potential of the Moab fault and its relation to salt tectonics in the Paradox Basin, Utah, in A. C. Huffman Jr., W. R. Lund, and L. H. Goodwin, eds., *Geology and resources of the Paradox Basin: Utah Geological Association Guidebook 25*, p. 251–264.
- Pevear, D., P. J. Vrolijk, and F. J. Lomgstaffe, 1997, Timing of Moab fault displacement and fluid movement integrated with burial history using radiometric and stable isotopes, in J. Hendry, P. Carey, J. Parnell, A. Ruffel, and R. Worden, eds., *Migration and interaction in sedimentary basins and orogenic belts: Geofluids*, v. 2, p. 42–45.
- Pollard, D. D., and A. Aydin, 1988, Progress in understanding jointing over the past century: *Geological Society of America Bulletin*, v. 100, p. 1181–1204.
- Quinn, O. F., and R. S. Haszeldine, 2004, Quartz cementation of a faulted sandstone at shallow burial: Petrographic and poroperm data: United Kingdom North Sea (extended abs.): *AAPG Hedberg Research Conference: Structural diagenesis: Fundamental advances and new applications from a holistic view of mechanical and chemical processes*, Austin, Texas: AAPG Search and Discovery Article 90027: <http://www.searchanddiscovery.net/documents/hedberg2004austin/index.htm>.
- Robinson, N. I., J. M. Sharp Jr., and I. Kreisel, 1998, Contaminant transport in sets of parallel finite fractures with fracture skins: *Journal of Contaminant Hydrology*, v. 31, p. 83–109, doi:10.1016/S0169-7722(97)00055-7.
- Shawe, D. R., 1976, Sedimentary rock alteration in the Slick Rock district, San Miguel and Dolores Counties, Colorado: *U.S. Geological Survey Professional Paper No. 576-D*, 51 p.
- Shipton, Z. K., J. P. Evans, D. Kirschner, P. T. Kolesar, A. P. Williams, and J. Heath, 2004, Analysis of CO₂ leakage through “low-permeability” faults from natural reservoirs in the Colorado Plateau, east-central Utah: *Geological Society Special Publications 233*, p. 43–58.
- Solum, J. G., B. A. van der Pluijm, and D. R. Peacor, 2005, Neocrystallization, fabrics and age of clay minerals from an exposure of the Moab fault, Utah: *Journal of Structural Geology*, v. 27, p. 1563–1576, doi:10.1016/j.jsg.2005.05.002.
- Spangler, L. E., D. L. Naftz, and Z. E. Peterman, 1996, Hydrology, chemical quality, and characterization of salinity in the Navajo aquifer in and near the Greater Aneth oil field, San Juan County, Utah: *U.S. Geological Survey Water-Resources Investigations Report 96-4155*, 90 p.
- Surdam, R. C., and L. J. Crossey, 1985, Mechanisms of organic/inorganic interactions in sandstone/shale sequences, in D. L. Gautier, Y. K. Kharaka, and R. C. Surdam, eds., *Relationship of organic matter and mineral diagenesis: SEPM Short Course 17*, p. 177–232.
- Tuccillo, M. E., I. M. Cozzarelli, and J. S. Herman, 1999, Iron reduction in the sediments of a hydrocarbon-contaminated aquifer: *Applied Geochemistry*, v. 14, p. 71–83.
- Turner, P., 1980, *Continental red beds: Developments in sedimentology*: Amsterdam, Elsevier, v. 29, 562 p.

- Vrolijk, P., and B. A. van der Pluijm, 1999, Clay gouge: *Journal of Structural Geology*, v. 21, p. 1039–1048, doi:[10.1016/S0191-8141\(99\)00103-0](https://doi.org/10.1016/S0191-8141(99)00103-0).
- Walker, T. R., 1975, Red beds in the western interior of the United States: U.S. Geological Survey Professional Paper No. 853, part II, p. 49–56.
- Walker, T. R., B. Waugh, and A. J. Grone, 1978, Diagenesis in first-cycle desert alluvium of Cenozoic age, southwestern United States and northwestern Mexico: *Geological Society of America Bulletin*, v. 89, p. 19–32, doi:[10.1130/0016-7606\(1978\)89<19:DIFDAO>2.0.CO;2](https://doi.org/10.1130/0016-7606(1978)89<19:DIFDAO>2.0.CO;2).
- Watson, J. S., D. M. Jones, R. P. J. Swannell, and A. C. T. van Duin, 2002, Formation of carboxylic acids during aerobic biodegradation of crude oil and evidence of microbial oxidation of hopanes: *Organic Geochemistry*, v. 33, p. 1153–1169, doi:[10.1016/S0146-6380\(02\)00086-4](https://doi.org/10.1016/S0146-6380(02)00086-4).
- Yielding, G., B. Freeman, and D. T. Needham, 1997, Quantitative fault seal prediction: *AAPG Bulletin*, v. 81, p. 897–917.